

**$\Lambda_c$  BARYON PRODUCTIONS IN EFFECTIVE  
LAGRANGIAN APPROACH**



**A Thesis Submitted in Partial Fulfillment of the Requirements for the  
Degree of Doctor of Philosophy in Physics  
Suranaree University of Technology  
Academic Year 2020**

# การผลิตเบร็ออนชนิดแลมด้าซีด้วยวิธีการลากรานเจียนยังผล

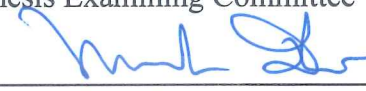


วิทยานิพนธ์นี้เป็นส่วนหนึ่งของการศึกษาตามหลักสูตรปริญญาวิทยาศาสตรดุษฎีบัณฑิต  
สาขาวิชาฟิสิกส์  
มหาวิทยาลัยเทคโนโลยีสุรนารี  
ปีการศึกษา 2563

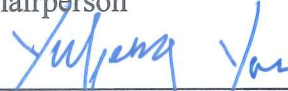
**$\Lambda_c$  BARYON PRODUCTIONS  
IN EFFECTIVE LAGRANGIAN APPROACH**

Suranaree University of Technology has approved this thesis submitted in partial fulfillment of the requirements for the Degree of Doctor of Philosophy.


Thesis Examining Committee

  
\_\_\_\_\_  
(Assoc. Prof. Dr. Panomsak Meemon)

Chairperson

  
\_\_\_\_\_  
(Prof. Dr. Yupeng Yan)

Member (Thesis Advisor)

  
\_\_\_\_\_  
(Prof. Dr. Atsushi Hosaka)

Member (Thesis Co-Advisor)

  
\_\_\_\_\_  
(Asst. Prof. Dr. Khanchai Khosonthongkee)


Member

  
\_\_\_\_\_  
(Dr. Daris Samart)

Member (Thesis Co-Advisor)

  
\_\_\_\_\_  
(Dr. Nopmanee Supanam)

Member (Thesis Co-Advisor)

  
\_\_\_\_\_  
(Prof. Dr. Santi Maensiri)

  
\_\_\_\_\_  
(Assoc. Prof. Dr. Chatchai Jothityangkoon)

Vice Rector for Academic Affairs  
and Quality Assurance

Dean of Institute of Science

รณัษ สังกะกะฤกษ์ : การผลิตแบรีออนชนิดเลมด้าซีด้วยวิธีการลากรานเจียนยังผล  
( $\Lambda_c$  BARYON PRODUCTIONS IN EFFECTIVE LAGRANGIAN APPROACH)  
อาจารย์ที่ปรึกษา : ศาสตราจารย์ ดร.ยูเป็ง แยน, 86 หน้า

ลากรานเจียนยังผลสำหรับดีเมซอน แบรีออนที่ประกอบด้วยชาร์มควาร์ก และแบรีออนที่ประกอบด้วยควาร์กเบา ได้ถูกสร้างขึ้น ที่อันดับไครอล  $\mathcal{O}(q^0)$  และ  $\mathcal{O}(q)$  ลากรานเจียนที่ทั่วไปที่สุดนั้นประกอบด้วยเทอมทางคณิตศาสตร์จำนวน 15 เทอม เพื่อเพิ่มขีดความสามารถในการทำนายของแบบจำลองที่ได้สร้างขึ้นมา สมมาตรควาร์กหนักและการวิเคราะห์เอ็นซีขนาดใหญ่อิงถูกนำมาใช้ในการลดจำนวนตัวแปรอิสระของแบบจำลอง ด้วยเหตุนี้ จำนวนตัวแปรอิสระลดลงเหลือจำนวน 5 เทอม โดยการศึกษาการสลายตัวของแบรีออนชนิด  $\Lambda_c$  และ  $\Sigma_c$  ด้วยวิธีการลากรานเจียนยังผลและแบบจำลองควาร์ก ค่าคงที่คู่ควบบางตัวสำหรับลากรานเจียนยังผลจึงได้รับการประเมิน จากนั้น ปฏิบัติการผลิตแบรีออนที่ประกอบด้วยสเตรนจ์ควาร์กและแบรีออนที่ประกอบด้วยชาร์มควาร์กจากการประลัยระหว่าง โปรตอน-แอนติโปรตอนได้ถูกศึกษาด้วยทฤษฎีลากรานเจียนยังผลและทฤษฎีเรจเจ จากการวิเคราะห์พบว่า อัตราการผลิตแบรีออนที่ประกอบด้วยชาร์มควาร์กมีค่าเป็น  $10^{-4}$  ถึง  $10^{-5}$  เท่าของอัตราการผลิตแบรีออนที่ประกอบด้วยสเตรนจ์ควาร์ก

มหาวิทยาลัยเทคโนโลยีสุรนารี

สาขาวิชาฟิสิกส์  
ปีการศึกษา 2563

ลายมือชื่อนักศึกษา T. Sangkhakrit  
ลายมือชื่ออาจารย์ที่ปรึกษา Jupung Yan  
ลายมือชื่ออาจารย์ที่ปรึกษาร่วม Alphab  
ลายมือชื่ออาจารย์ที่ปรึกษาร่วม Daris Samgait  
ลายมือชื่ออาจารย์ที่ปรึกษาร่วม Bunl ๑๗.

THANAT SANGKHAKRIT :  $\Lambda_c$  BARYON PRODUCTIONS IN  
EFFECTIVE LAGRANGIAN APPROACH.

THESIS ADVISOR : PROF. YUPENG YAN, Ph.D. 86 PP.

CHARMED BARYONS/EFFECTIVE LAGRANGIAN/HEAVY QUARK  
SYMMETRY/LARGE- $N_c$  ANALYSIS/QUARK MODEL/REGGE APPROACH

Effective Lagrangians for  $D$ -meson, charmed, and light baryons are constructed. At the chiral orders  $\mathcal{O}(q^0)$  and  $\mathcal{O}(q)$ , the most general Lagrangian is contributed by fifteen terms. To make our model more predictive, heavy quark symmetry and large- $N_c$  analysis are employed to derive sum rules for the unknown coupling constants. As a result, the number of free parameters is then reduced to five. By investigating various decays of  $\Lambda_c$  and  $\Sigma_c$  baryons in effective Lagrangian method and quark model, some coupling constants are estimated. Then, we employ effective Lagrangian and Regge approaches to study various strangeness and charm productions from proton-antiproton collisions. From our analyses, production rates of charmed baryons are typically  $10^{-4}$  to  $10^{-5}$  times those of strange baryons.

School of Physics

Academic Year 2020

Student's Signature T. Sangkhakrit  
Advisor's Signature Yupeng Yan  
Co-Advisor's Signature Abhishek  
Co-Advisor's Signature Daris Samart  
Co-Advisor's Signature Wit J.

# ACKNOWLEDGEMENTS

First of all, I would like to express my gratitude to my thesis advisor, Prof. Dr. Yupeng Yan, who has provided me with great guidance and encouragement throughout my research, as well as to my co-advisors, Dr. Daris Samart and Dr. Nopmanee Supanam, who have continuously supported me with their patience and understanding. I am also grateful to Prof. Dr. Atsushi Hosaka, my international co-advisor, who has provided me with his patient guidance and the opportunity to continue my research at RCNP, Osaka University.

I would also like to thank the thesis committee members, including Assoc. Prof. Dr. Panomsak Meemon and Asst. Prof. Dr. Khanchai Khosonthongkee, for their encouragement and valuable feedback.

My colleagues in the Nuclear and Particle Physics group at Suranaree University of Technology, particularly Dr. Kai Xu, Mr. Attaphon Kaewsnod, and Mr. Zheng Zhao, have provided me with continuous support throughout my Ph.D. study. Additionally, I am grateful to all the staff and members in the RCNP theory group, particularly Dr. Sang-In Shim, Dr. Denny Lane B. Sombillo, and Dr. Ahmad Jafar Arifi, for their useful feedback and discussions.

This work is supported by the Thailand Science Research and Innovation and Suranaree University of Technology through the Royal Golden Jubilee Ph.D. Program (Grant No.PHD/0041/2555), Center of Excellence in High Energy Physics and Astrophysics, Suranaree University of Technology, RCNP, Osaka University, and FrontierLab Mini program, Osaka University.

Finally, I am grateful to my family for their support and understanding.

Thanat Sangkhakrit

# CONTENTS

	<b>Page</b>
ABSTRACT IN THAI . . . . .	I
ABSTRACT IN ENGLISH . . . . .	II
ACKNOWLEDGEMENTS . . . . .	III
CONTENTS . . . . .	IV
LIST OF TABLES . . . . .	VII
LIST OF FIGURES . . . . .	VIII
<b>CHAPTER</b>	
<b>I INTRODUCTION . . . . .</b>	<b>1</b>
<b>II CONSTRUCTION OF THE EFFECTIVE LAGRANGIANS</b>	<b>5</b>
2.1 Symmetries of QCD and effective Lagrangian approach . . . . .	5
2.2 Building blocks . . . . .	8
2.3 Effective Lagrangians . . . . .	11
<b>III DETERMINATION OF COUPLING CONSTANTS IN HEAVY QUARK SYMMETRY AND LARGE-<math>N_c</math> ANALYSIS</b>	<b>13</b>
3.1 Heavy quark symmetry . . . . .	14
3.1.1 Introduction . . . . .	14
3.1.2 Building blocks of the heavy quark effective field theory . . .	16
3.1.3 Heavy quark spin invariant effective Lagrangians . . . . .	18
3.1.4 $1/m_Q$ expansion . . . . .	19
3.1.5 Results . . . . .	21

## CONTENTS (Continued)

	Page
3.2 Large- $N_c$ picture . . . . .	21
3.2.1 Introduction . . . . .	21
3.2.2 $1/N_c$ expansion . . . . .	23
3.2.3 Results . . . . .	26
3.3 Combining heavy quark and large- $N_c$ constraints . . . . .	26
<b>IV ESTIMATION OF COUPLING CONSTANTS IN QUARK MODEL . . . . .</b>	<b>27</b>
4.1 Feynman amplitudes . . . . .	27
4.2 Quark model . . . . .	30
4.3 Results . . . . .	33
<b>V PRODUCTIONS OF STRANGE AND CHARMED BARYONS IN EFFECTIVE LAGRANGIAN AND REGGE APPROACHES . . . . .</b>	<b>36</b>
5.1 Introduction . . . . .	37
5.2 Unitarity . . . . .	39
5.3 Effective Lagrangian approach . . . . .	41
5.3.1 Feynman amplitudes . . . . .	41
5.3.2 Results for strangeness productions . . . . .	45
5.3.3 Predictions for charm productions . . . . .	48
5.4 Regge approach . . . . .	51
5.4.1 Amplitudes . . . . .	51
5.4.2 Results for strangeness productions . . . . .	54



## CONTENTS (Continued)

	Page
5.4.3 Predictions for charm productions . . . . .	55
5.5 Total cross sections . . . . .	55
<b>VI SUMMARY . . . . .</b>	<b>58</b>
REFERENCES . . . . .	61
APPENDICES	
APPENDIX A CHIRAL POWER COUNTING OF MATTER FIELDS	76
APPENDIX B ISOSPIN MATRICES . . . . .	79
APPENDIX C REGGE PARAMETERS . . . . .	81
C.1 Regge trajectories . . . . .	81
C.2 Scaling parameters . . . . .	83
CURRICULUM VITAE . . . . .	86

# LIST OF TABLES

Table		Page
4.1	The flavor-spin-color factors $C_i$ corresponding to the decay processes $B_c \rightarrow B\phi_c$ . . . . .	33
4.2	Coupling constants of $D$ -meson, charmed, and light baryons from our estimation. The numbers in the brackets denote the magnitudes of the original coupling constants used in the cited literature ([a] (Kim et al., 2015), [b] (Sangkhakrit et al., 2022), [c] (Khodjamirian et al., 2012), [d] (Titov and Kampf, 2008), [e] (Azizi et al., 2015a), [f] (Azizi et al., 2014), [g] (Fontoura et al., 2017), [h] (Azizi et al., 2015b), [i] (Yu et al., 2019)), if available. . . . .	34
C.1	Parameters of corresponding meson trajectories for strangeness and charm productions from $p\bar{p}$ reactions . . . . .	83

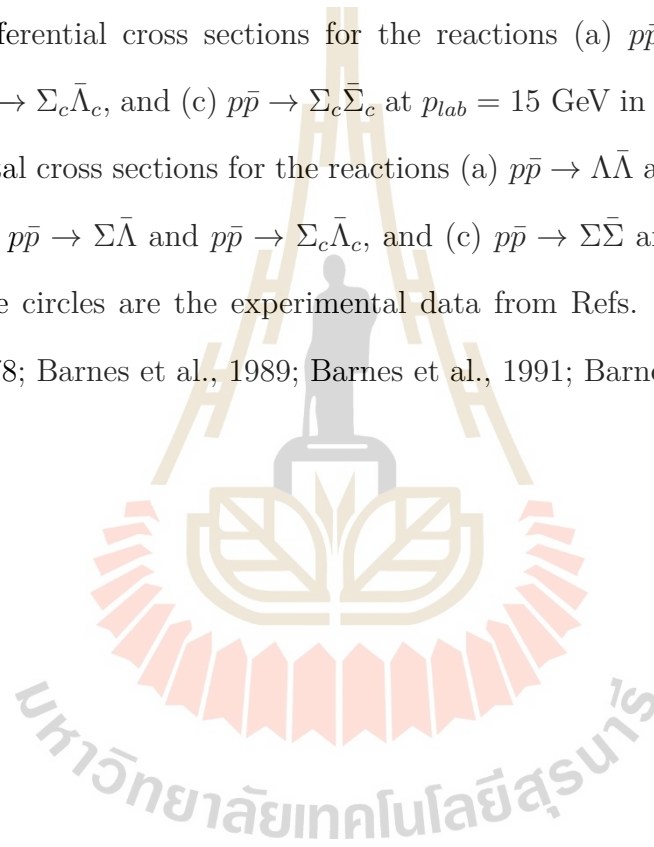


# LIST OF FIGURES

Figure		Page
4.1	Feynman diagram for the decay process $B_c(p, s) \rightarrow B(k, s') \phi_c(q, s'')$ .	28
4.2	Schematic diagram for the decay process $B_c \rightarrow B \phi_c$ in ${}^3P_0$ quark model. The bottom quark line is that of charm quark while the rest are those of $u$ and $d$ quarks. . . . .	31
5.1	Tree-level diagram for the reaction $p\bar{p} \rightarrow Y\bar{Y}'$ . . . . .	41
5.2	Tree-level diagram for the reaction $p\bar{p} \rightarrow Y_c\bar{Y}'_c$ . . . . .	44
5.3	Differential cross sections for the reaction $p\bar{p} \rightarrow \Lambda\bar{\Lambda}$ at $p_{lab} = 6$ GeV in the effective Lagrangian model. The circles denote the experimental data from Ref. (Becker et al., 1978). . . . .	47
5.4	Differential cross sections for the reaction $p\bar{p} \rightarrow \Sigma\bar{\Lambda}$ at $p_{lab} = 6$ GeV in the effective Lagrangian model. The circles denote the experimental data from Ref. (Becker et al., 1978). . . . .	47
5.5	Differential cross sections for the reaction $p\bar{p} \rightarrow \Sigma\bar{\Sigma}$ at $p_{lab} = 6$ GeV in the effective Lagrangian model. . . . .	48
5.6	Differential cross sections for the reaction $p\bar{p} \rightarrow \Lambda_c\bar{\Lambda}_c$ at $p_{lab} = 15$ GeV in the effective Lagrangian model. . . . .	49
5.7	Differential cross sections for the reaction $p\bar{p} \rightarrow \Sigma_c\bar{\Lambda}_c$ at $p_{lab} = 15$ GeV in the effective Lagrangian model. . . . .	49
5.8	Differential cross sections for the reaction $p\bar{p} \rightarrow \Sigma_c\bar{\Sigma}_c$ at $p_{lab} = 15$ GeV in the effective Lagrangian model. . . . .	49

## LIST OF FIGURES (Continued)

<b>Figure</b>		<b>Page</b>
5.9	Differential cross sections for the reactions (a) $p\bar{p} \rightarrow \Lambda\bar{\Lambda}$ , (b) $p\bar{p} \rightarrow \Sigma\bar{\Lambda}$ , and (c) $p\bar{p} \rightarrow \Sigma\bar{\Sigma}$ at $p_{lab} = 6$ GeV in the Regge model. The circles denote the experimental data from Ref.(Becker et al., 1978).	54
5.10	Differential cross sections for the reactions (a) $p\bar{p} \rightarrow \Lambda_c\bar{\Lambda}_c$ , (b) $p\bar{p} \rightarrow \Sigma_c\bar{\Lambda}_c$ , and (c) $p\bar{p} \rightarrow \Sigma_c\bar{\Sigma}_c$ at $p_{lab} = 15$ GeV in the Regge model.	55
5.11	Total cross sections for the reactions (a) $p\bar{p} \rightarrow \Lambda\bar{\Lambda}$ and $p\bar{p} \rightarrow \Lambda_c\bar{\Lambda}_c$ , (b) $p\bar{p} \rightarrow \Sigma\bar{\Lambda}$ and $p\bar{p} \rightarrow \Sigma_c\bar{\Lambda}_c$ , and (c) $p\bar{p} \rightarrow \Sigma\bar{\Sigma}$ and $p\bar{p} \rightarrow \Sigma_c\bar{\Sigma}_c$ . The circles are the experimental data from Refs. (Becker et al., 1978; Barnes et al., 1989; Barnes et al., 1991; Barnes et al., 1996).	56



# CHAPTER I

## INTRODUCTION

The sophisticated dynamics of the strong interaction between quarks and gluons are described by the  $SU(3)$  gauge theory, known as Quantum Chromodynamics (QCD). Due to its non-Abelian nature, the strong interaction exhibits distinct behaviors at low and high energy regimes. At high energies, the interaction weakens, enabling its investigation through perturbative QCD. Conversely, perturbative QCD fails to hold in the low energy region, where the coupling constant becomes large. Non-perturbative QCD introduces an alternative running behavior for the strong coupling constant. Among the most remarkable non-perturbative phenomena is color confinement, wherein quarks and gluons combine to form observable colorless hadrons.

Physics of hadrons containing charm quarks, or in general heavy quarks has been one of actively studied subjects in hadron physics since the first observations of  $J/\psi$  meson in 1974 (Augustin et al., 1974; Aubert et al., 1974) and of the charmed baryon states ( $\Sigma_c, \Lambda_c$ ) in 1975 (Cazzoli et al., 1975). Particularly, various exotic hadrons have been observed by Belle, BABAR, BESIII, and LHCb collaborations in the 21st century (Choi et al., 2003; Aubert et al., 2005a; Aubert et al., 2005b; Abe et al., 2007; Choi et al., 2008; Hosaka et al., 2016; Ablikim et al., 2013a; Liu et al., 2013; Ablikim et al., 2013b; Aaij et al., 2013; Aaij et al., 2014). Accordingly, theoretical studies have been extensively performed in various QCD inspired approaches such as the quark model (Micu, 1969; Godfrey and Isgur, 1985; Maiani et al., 2005; Ebert et al., 2006; Limphirat et al., 2010; Xu et al.,

2020), models of chiral and heavy quark symmetries (Gupta and Johnson, 1995; Ebert et al., 1998; Glozman, 2004; Nowak et al., 2004; AlFiky et al., 2006; Liu et al., 2006), non-relativistic QCD (Brambilla et al., 2000; Braguta et al., 2005), and the first principle calculations of lattice QCD (Isgur and Paton, 1985; Chen, 2001; Okamoto et al., 2002; Liao and Manke, 2002; McNeile et al., 2002; Chiu and Hsieh, 2006; Chiu and Hsieh, 2007) (See Refs. (Swanson, 2006; Brambilla et al., 2011) for reviews). Structure and decays are mostly focused while productions are less investigated according to their inclusive nature. Physically, the production mechanism of heavy quarks from the light quarks in the initial state is an interesting and the least understood issue. Quantitative descriptions of such heavy quark productions in exclusive processes provide a better understanding of the non-perturbative dynamics of QCD and the structure of the hadrons.

As an example of an exclusive process, a pion induced reaction for charmed baryon production was studied many years ago at Brookhaven (Christenson et al., 1985), which reported only null results. An updated experiment is planned at J-PARC and the construction of the facility is ongoing (Morino et al., 2012), and the corresponding theoretical studies have been also carried out (Kim et al., 2015; Kim et al., 2016; Shim et al., 2019; Shim et al., 2020). In this thesis, we study another process induced by antiprotons. This is a planned experiment at GSI as  $\bar{P}$ ANDA project of FAIR, providing another promising reactions to produce charmed baryons. At the same time, strange hyperons can also be produced, so we can study systematically both strange and charm productions.

By now several models for charm productions have been proposed and cross sections have been computed. In Ref. (Kroll et al., 1989), various charm production cross sections have been estimated in the quark-diquark picture. In this model, charmed hadrons are produced via the interaction between the active

constituents (quark or diquark) of the initial states. This approach has some similarity to the handbag approach used in Ref. (Goritschnig et al., 2009). In this case, the transition amplitude of the reaction  $p\bar{p} \rightarrow \Lambda_c\bar{\Lambda}_c$  is computed in terms of the amplitude for the hard subprocess (i.e.,  $u\bar{u} \rightarrow c\bar{c}$ ) and the soft hadronic matrix elements for  $p \rightarrow \Lambda_c$  and  $\bar{p} \rightarrow \bar{\Lambda}_c$  transitions. Quark-Gluon String Model (QGSM) and Regge approach are employed by several authors in Refs. (Kaidalov and Volkovitsky, 1994; Titov and Kampfer, 2008; Khodjamirian et al., 2012). In this model, the annihilation of  $q\bar{q}$  pair from the initial states is followed by the formation of the intermediate string, then the observed charmed hadrons are consequently produced from the string fission. Meson-exchange framework was employed in Refs. (Haidenbauer et al., 1992; Haidenbauer and Krein, 2017) to compute  $\Lambda_c\bar{\Lambda}_c$  production cross sections. This model was developed from Jülich meson-baryon model, which is originally employed to compute the cross sections for the reaction  $p\bar{p} \rightarrow \Lambda\bar{\Lambda}$  within the coupled-channel framework. Effective Lagrangian approach with coupling constants from  $SU(4)$  symmetry is employed in Ref. (Shyam and Lenske, 2014) to compute various charm productions, which are produced via  $D$  and  $D^*$  meson-exchange processes. From these studies, the strong model dependence is exhibited since the predicted charm production cross sections are different by several orders.

This thesis focuses on the investigation of charm productions using the effective Lagrangian approach, incorporating constraints derived from heavy quark symmetry and large- $N_c$  analysis. Furthermore, we estimate various coupling constants within the  $^3P_0$  quark model. Additionally, we introduce a second model based on the Regge approach, enabling the analysis of strangeness productions and the prediction of production rates for charmed baryons. Since the Regge approach is applicable in the diffractive region, we also utilize the effective La-

grangian method to examine the same processes. As a result, a description of the production rates in the proximity of the threshold is also provided.

The content of this thesis is organized as follows: In Chapter II, effective Lagrangians for  $D$ -mesons, charmed, and light baryons are constructed, establishing a theoretical framework for their description. Chapter III focuses on reducing the number of independent model parameters through the application of heavy quark symmetry and large- $N_c$  analysis. In Chapter IV, the estimation of coupling constants is conducted by investigating various decay modes of  $\Lambda_c$  and  $\Sigma_c$  baryons in effective Lagrangian method and quark model. Chapter V investigates strangeness and charm productions using effective Lagrangian and Regge approaches. Model parameters will be determined through a fitting procedure, incorporating existing data on strangeness productions and utilizing the Quark Gluon String Model (QGSM). Predictions for the production rates of various charmed baryons will be generated and compared with those of strange baryons. Finally, Chapter VI provides a comprehensive summary and conclusion for this thesis. By following this systematic structure, we aim to advance the understanding of the properties of charmed baryons, contributing to the broader field of hadron physics.



# CHAPTER II

## CONSTRUCTION OF THE EFFECTIVE LAGRANGIANS

In this chapter, we present an overview of the fundamental principles governing the formulation of an effective Lagrangian method. The discussion commences with a detailed examination of the symmetries of QCD, followed by a concise review of the effective Lagrangian method. Next, we discuss the building blocks of the most general Lagrangian and their corresponding transformations. Subsequently, we construct the effective Lagrangians necessary for calculating charm production rates. For further insights into this subject, we refer the interested reader to the Refs. (Koch, 1997; Machleidt and Entem, 2011; Scherer and Schindler, 2012).

### 2.1 Symmetries of QCD and effective Lagrangian approach

The strong interaction between quarks and gluons is described by the QCD Lagrangian,

$$\mathcal{L} = -\frac{1}{4}F_{\mu\nu}^a F^{a\mu\nu} + \bar{\psi} (i\not{D} - M) \psi, \quad (2.1)$$

with

$$D_\mu = \partial_\mu - \frac{g_s}{2} G_\mu^a \lambda^a, \quad (2.2)$$

$$F_{\mu\nu}^a = \partial_\mu G_\nu^a - \partial_\nu G_\mu^a + g_s f^{abc} G_\mu^b G_\nu^c. \quad (2.3)$$

Here,  $\psi$  and  $M$  denote quark fields and the mass matrix, while  $G_\mu^a$  are eight gluon fields. The strengths of quark-gluon and gluon-gluon interactions are expressed by the strong coupling constant  $g_s$ . This Lagrangian exhibits  $C$ ,  $P$ , and  $T$  symmetries separately as well as  $SU(3)$  color symmetry. In addition, different symmetries in the flavor space are also held by strong interactions.

In this work, the physics of the two lightest quarks ( $u$  and  $d$ ) and charm quark ( $c$ ) is mainly focused. Therefore, the corresponding Lagrangian of massless two quark flavors ( $u$  and  $d$ ) is given as

$$\mathcal{L}_0 = i\bar{\psi}^k \not{\partial} \psi^k, \quad (2.4)$$

where  $\psi = \begin{pmatrix} \psi^1 \\ \psi^2 \end{pmatrix} = \begin{pmatrix} \psi^u \\ \psi^d \end{pmatrix}$  and  $\not{\partial} = \partial_\mu \gamma^\mu$ . Since gluon fields are not participate in the chiral transformations, they can be neglected in our present discussion. By utilizing the following transformations of the helicity eigenstates  $\psi_L$  and  $\psi_R$  (i.e.,  $\psi_{L,R} = P_{L,R}\psi = \frac{1}{2}(1 \mp \gamma_5)\psi$ ),

$$\begin{aligned} \psi_L &\rightarrow \psi'_L = e^{-\frac{i}{2}(\boldsymbol{\tau} \cdot \boldsymbol{\theta}_L)} \psi_L, \\ \psi_R &\rightarrow \psi'_R = e^{-\frac{i}{2}(\boldsymbol{\tau} \cdot \boldsymbol{\theta}_R)} \psi_R, \end{aligned} \quad (2.5)$$

where  $\boldsymbol{\tau}$  are Pauli isospin matrices while  $\boldsymbol{\theta}_{L,R}$  are arbitrary parameters. We can show that the Lagrangian  $\mathcal{L}_0$  is invariant under these transformations, in which the corresponding symmetry group is  $SU(2)_L \times SU(2)_R$ . The corresponding conserved currents are

$$J_{L,R}^{k\mu} = \bar{\psi}_{L,R} \gamma^\mu \frac{\tau_k}{2} \psi_{L,R} \quad (k = 1, 2, 3), \quad (2.6)$$

From these currents, one can introduce the following combinations,

$$J_V^{k\mu} = J_R^{k\mu} + J_L^{k\mu}, \quad (2.7)$$

$$J_A^{k\mu} = J_R^{k\mu} - J_L^{k\mu}. \quad (2.8)$$

As a result, the transformations for quark doublet under  $SU(2)_V \times SU(2)_A$  group are written as,

$$\begin{aligned} \psi &\rightarrow \psi' = e^{-\frac{i}{2}\boldsymbol{\tau}\cdot\boldsymbol{\theta}_V} \psi, \\ \psi &\rightarrow \psi' = e^{-\frac{i}{2}\boldsymbol{\gamma}_5\boldsymbol{\tau}\cdot\boldsymbol{\theta}_A} \psi. \end{aligned} \quad (2.9)$$

This concludes that massless QCD in the presence of the two light quark flavors is invariant under  $SU(2)_V \times SU(2)_A$  chiral symmetry. Compared to the typical energy scales of QCD, the masses of  $u$  and  $d$  quarks are smaller. This means, chiral symmetry is held only for those in the light quark sector. Therefore, if we consider that charm quark is sufficiently heavy in the very low energy domain of interest, only  $u$  and  $d$  quarks are involved.

Effective Lagrangian approach is by now an efficient method to investigate the low-energy dynamics of the strong interaction. This method was firstly introduced in the published article of Weinberg (Weinberg, 1979). And then, it was consequently developed by Gasser and Leutwyler (Gasser and Leutwyler, 1984; Gasser, 1987). In this framework, effective Lagrangians are constructed from the chosen degrees of freedom in a particular low-energy domain of interest, where the symmetries of the original theory are kept. Typically, relevant degrees of freedom in low-energy hadron physics are mesons and baryons instead of quarks and gluons. Then, one is able to calculate physical observables in terms of an expansion in  $q/\Lambda$ . The cutoff parameter  $\Lambda$  is of the order 1 GeV and the parameter  $q$  denotes small energy, momenta, or masses. As  $q \ll \Lambda$ , the most general Lagrangian is only contributed by a finite number of terms, each of them is consisted by relevant field operators and an unknown coupling constant. In principle,

these coupling constants should be calculable from QCD inspired approaches (e.g., quark model, QCD sum rules). Otherwise, we need to determine them from the fit with the experimental data. Once these parameters has been determined, the predictive power of the effective Lagrangian theory is realized. Predictions from this approach are mostly consistent with the data near the production thresholds.

For instance, if chiral symmetry of massless two-flavor QCD is spontaneously broken to  $SU(2)_V$  group by the vacuum expectation value of quark bilinears, three massless Nambu Goldstone bosons are subsequently created. In this case, they are three isovector pions. This means, the spontaneous chiral symmetry breaking allows us to investigate various properties of Goldstone boson interactions, which are described in the framework of chiral perturbation theory (ChPT). The observables can be expanded in terms of  $\frac{q}{\Lambda_\chi}$ , where the small momenta of the Goldstone boson fields is denoted by  $q$  while  $\Lambda_\chi \equiv 4\pi F_\pi \approx 1.17$  GeV ( $F_\pi = 93$  MeV) is the chiral symmetry breaking scale.

## 2.2 Building blocks

In this section, we introduce relevant degrees of freedom required for the construction of the effective Lagrangians: D-mesons ( $D(1868)$ ,  $D^*(2009)$ ), charmed baryons ( $\Lambda_c(2286)$ ,  $\Sigma_c(2455)$ ,  $\Sigma_c(2520)$ ), and light baryons ( $N(939)$ ,  $\Delta(1232)$ ). In this notation, the average masses of these particles are displayed in the brackets. The corresponding isospin multiplets for these degrees of freedom are written as,

$$I = 0: \Lambda_c = \Lambda_c^+, \quad (2.10)$$

$$I = \frac{1}{2}: N = \begin{pmatrix} p \\ n \end{pmatrix}, \bar{D} = \begin{pmatrix} \bar{D}^0 \\ D^- \end{pmatrix}, \bar{D}^* = \begin{pmatrix} \bar{D}^{*0} \\ D^{*-} \end{pmatrix}, \quad (2.11)$$

$$I = 1: \Sigma_c = \begin{pmatrix} \Sigma_c^{++} \\ \Sigma_c^+ \\ \Sigma_c^0 \end{pmatrix}, \Sigma_c^* = \begin{pmatrix} \Sigma_c^{*++} \\ \Sigma_c^{*+} \\ \Sigma_c^{*0} \end{pmatrix}, \quad (2.12)$$

$$I = \frac{3}{2}: \Delta = \begin{pmatrix} \Delta^{++} \\ \Delta^+ \\ \Delta^0 \\ \Delta^- \end{pmatrix}, \quad (2.13)$$

where we have used  $D^* = D^*(2009)$  and  $\Sigma_c^* = \Sigma_c(2520)$ . For the isotriplet state  $\Sigma_c$  (as for  $\Sigma_c^*$ ), one can construct  $SU(2)$  adjoint representations in terms of the three dimensional basis composed by relevant isospin matrices. There are two different representations of the  $\Sigma_c$  state (as for  $\Sigma_c^*$ ): The  $2 \times 2$  matrix  $\Sigma_c^{(t)}$  and the  $4 \times 2$  matrix  $\Sigma_c^{(T)}$ . The first representation is appropriate for the couplings with the isodoublet states. On the other hand, the second one is used in those contributed by the isobar state  $\Delta$ . The explicit forms for  $\Sigma_c^{(t)}$  and  $\Sigma_c^{(T)}$  matrices will be discussed in the Appendix B. The  $SU(2)$  isospin rotations for these multiplets are summarized by

$$\Lambda_c \rightarrow \Lambda_c,$$

$$N \rightarrow e^{-i\alpha \cdot \mathbf{J}} N,$$

$$\bar{D} \rightarrow e^{-i\alpha \cdot \mathbf{J}} \bar{D},$$

$$\bar{D}^* \rightarrow e^{-i\alpha \cdot \mathbf{J}} \bar{D}^*,$$

$$\Sigma_c^{(t)} \rightarrow e^{-i\alpha \cdot \mathbf{J}} \Sigma_c^{(t)} e^{i\alpha \cdot \mathbf{J}},$$

$$\Sigma_c^{(T)} \rightarrow e^{-i\alpha \cdot \mathbf{J}} \Sigma_c^{(T)} e^{i\alpha \cdot \mathbf{J}},$$

$$\begin{aligned}
\Sigma_c^{*(t)} &\rightarrow e^{-i\boldsymbol{\alpha}\cdot\mathbf{J}}\Sigma_c^{*(t)}e^{i\boldsymbol{\alpha}\cdot\mathbf{J}}, \\
\Sigma_c^{*(T)} &\rightarrow e^{-i\boldsymbol{\alpha}\cdot\mathcal{J}}\Sigma_c^{*(T)}e^{i\boldsymbol{\alpha}\cdot\mathcal{J}}, \\
\Delta &\rightarrow e^{-i\boldsymbol{\alpha}\cdot\mathcal{J}}\Delta,
\end{aligned} \tag{2.14}$$

where  $\boldsymbol{\alpha} = (\alpha_1, \alpha_2, \alpha_3)$  are three arbitrary constants while  $\mathbf{J}$  and  $\mathcal{J}$  are isospin- $\frac{1}{2}$  and isospin- $\frac{3}{2}$  representations of  $SU(2)$  generators respectively.

Under the spontaneous chiral symmetry breaking, the transformation rules for these matter fields are not fixed, as they are related with each other by redefinitions of the fields. For this reason, we introduce a field  $u$  as a unitarity square root of the Goldstone boson field, i.e.,  $u^2 = U$ . The chiral transformation of the effective field  $u$  is

$$u \rightarrow \sqrt{h_R U h_L^\dagger} = h_R u \mathcal{K}^\dagger(h_L, h_R, U) = \mathcal{K}(h_L, h_R, U) u h_L^\dagger, \tag{2.15}$$

where  $h_R \in SU(2)_R$  and  $h_L \in SU(2)_L$ . The function  $\mathcal{K}(h_L, h_R, U)$  denotes the compensator field of the nonlinear chiral representation. The  $SU(2)_L \times SU(2)_R$  chiral transformations for the associated matter fields are therefore written as

$$\begin{aligned}
\Lambda_c &\rightarrow \Lambda_c, \\
N &\rightarrow \mathcal{K}N, \\
\bar{D} &\rightarrow \mathcal{K}\bar{D}, \\
\bar{D}^* &\rightarrow \mathcal{K}\bar{D}^*, \\
\boldsymbol{\tau} \cdot \boldsymbol{\Sigma}_c &\rightarrow \mathcal{K}\boldsymbol{\tau} \cdot \boldsymbol{\Sigma}_c \mathcal{K}^\dagger, \\
\boldsymbol{\tau} \cdot \boldsymbol{\Sigma}_c^* &\rightarrow \mathcal{K}\boldsymbol{\tau} \cdot \boldsymbol{\Sigma}_c^* \mathcal{K}^\dagger,
\end{aligned}$$

$$\Delta^{ijk} \rightarrow \mathcal{K}_i^i \mathcal{K}_m^j \mathcal{K}_n^k \Delta^{lmn}. \quad (2.16)$$

These transformations will be employed to construct effective Lagrangians for  $D$ -meson, charmed, and light baryons in the next section.

## 2.3 Effective Lagrangians

In this section, associated effective Lagrangians for  $D$ -meson, charmed, and light baryons are constructed. The corresponding chiral power counting rules for these degrees of freedom will be discussed in Appendix A. These Lagrangians are demanded to be singlet under transformations in Eq. (2.14), Eq. (2.16), and those of Lorentz and QCD discrete symmetries. As a result, the effective Lagrangians for pseudoscalar  $D$ -meson, light, and charmed baryons are written as

$$\mathcal{L}_{D\Sigma_c N} = \frac{g_1}{m_D} \partial_\mu D \bar{\Sigma}_c^{(t)} \gamma^\mu \gamma_5 N + H.c.,$$

$$\mathcal{L}_{D\Lambda_c N} = -\frac{g_2}{m_D} \partial_\mu D \bar{\Lambda}_c \gamma^\mu \gamma_5 N + H.c.,$$

$$\mathcal{L}_{D\Sigma_c^* N} = \frac{g_3}{m_D} \partial_\mu D \bar{\Sigma}_c^{(t),\mu} N + H.c.,$$

$$\mathcal{L}_{D\Sigma_c \Delta} = \frac{g_4}{m_D} \partial_\mu D \bar{\Sigma}_c^{(T)} \Delta^\mu + H.c.,$$

$$\mathcal{L}_{D\Sigma_c^* N} = -\frac{g_5}{m_D} \partial_\mu D \bar{\Sigma}_c^{(T),\nu} \gamma^\mu \gamma_5 \Delta_\nu + H.c., \quad (2.17)$$

while those for vector  $D$ -meson, light and charmed baryons are written as

$$\mathcal{L}_{D^* \Sigma_c N} = f_1 D_\mu \bar{\Sigma}_c^{(t)} \gamma^\mu N + \frac{ih_1}{2m_D} D_{\mu\nu} \bar{\Sigma}_c^{(t)} \sigma^{\mu\nu} N + H.c.,$$

$$\mathcal{L}_{D^* \Lambda_c N} = f_2 D_\mu \bar{\Lambda}_c \gamma^\mu N - \frac{h_2}{2m_D} D_{\mu\nu} \bar{\Lambda}_c \sigma^{\mu\nu} N + H.c.,$$

$$\begin{aligned}
\mathcal{L}_{D^*\Sigma_c^*N} &= f_3 D_\mu \bar{\Sigma}_c^{(t),\mu} i\gamma_5 N - \frac{ih_3}{m_D} D_{\mu\nu} \bar{\Sigma}_c^{(t),\mu} \gamma^\nu \gamma_5 N + H.c., \\
\mathcal{L}_{D^*\Sigma_c\Delta} &= -f_4 D_\mu \bar{\Sigma}_c^{(T)} \gamma_5 \Delta^\mu + \frac{h_4}{m_D} D_{\mu\nu} \bar{\Sigma}_c^{(T)} \gamma^\mu \gamma_5 \Delta^\nu + H.c., \\
\mathcal{L}_{D^*\Sigma_c^*\Delta} &= -f_5 D_\mu \bar{\Sigma}_c^{(T),\nu} \gamma^\mu \Delta_\nu + \frac{h_5}{2m_D} D_{\mu\nu} \bar{\Sigma}_c^{(T),\mu} \Delta^\nu + H.c., \tag{2.18}
\end{aligned}$$

with

$$D_{\mu\nu} \equiv \partial_\mu D_\nu - \partial_\nu D_\mu. \tag{2.19}$$

Here,  $\tau$  matrices operate on the isospin states of  $N$  and  $D$  (or  $D^*$ ) while  $T$  matrices operate on those of  $\Delta$  and  $D$  (or  $D^*$ ). The coupling constants  $g$ ,  $f$ , and  $h$  are those of axial-vector, vector, and tensor couplings, respectively. The Lagrangians with the coupling constants  $f_3$  and  $f_4$  are of the chiral order  $\mathcal{O}(q)$ , while the remaining terms are of the order  $\mathcal{O}(q^0)$ .

We have constructed the effective Lagrangians for  $D$ -meson, charmed, and light baryons at the chiral orders  $\mathcal{O}(q^0)$  and  $\mathcal{O}(q)$ . As a consequence, the most general effective Lagrangian is contributed by the fifteen interacting Lagrangians in Eqs. (2.17) to (2.18). The reduction of model parameters by using heavy quark symmetry and large- $N_c$  analysis will be discussed in the next chapter.



# CHAPTER III

## DETERMINATION OF COUPLING CONSTANTS IN HEAVY QUARK SYMMETRY AND LARGE- $N_c$ ANALYSIS

In the previous chapter, we constructed effective Lagrangians for D-mesons, charmed hadrons, and light baryons, introducing fifteen independent parameters to our model. Since these Lagrangians involve charmed hadrons, it is appropriate to investigate their properties in the heavy quark limit. By constructing the most general heavy quark spin invariant effective Lagrangian and expanding our effective Lagrangians in powers of  $\frac{1}{m_Q}$ , the number of model parameters can be reduced by the constraints of heavy quark symmetry. Additional details can be found in Refs. (Yan et al., 1992; Wise, 1993; Neubert, 1994; Manohar and Wise, 2000). Furthermore, a spin-flavor symmetry of baryons emerges in the limit where the number of colors  $N_c$  is large (Lebed, 1999). Baryon matrix elements can then be systematically analyzed using  $\frac{1}{N_c}$  expansion, leading to constraints for the model parameters.

In this chapter, we present the reduction of model parameters. First, we reduce the number of free parameters by using heavy quark symmetry in the first section, and then by large- $N_c$  analysis in the second section. In this thesis, we focus on deriving heavy quark constraints while briefly reviewing those of large- $N_c$  analysis. Subsequently, the two sets of constraints are combined into combining heavy quark and large- $N_c$  constraints.

## 3.1 Heavy quark symmetry

### 3.1.1 Introduction

Compared to the typical scales of QCD (e.g.,  $\Lambda_\chi = 4\pi F_\pi \approx 1.17$  GeV), quarks are commonly divided into two sets: light quarks  $q = \{u, d, s\}$  and heavy quarks  $Q = \{c, b, t\}$ . The former set consists of quarks that are lighter than  $\Lambda_\chi$  while the heavier ones belong to the latter set. Since  $m_q \ll \Lambda_\chi$ , the properties of hadrons containing light quarks can be investigated by taking the limit  $m_q \rightarrow 0$ . The associated symmetry is the approximate  $SU(3)_L \times SU(3)_R$  chiral symmetry. On the other hand, the heavy quark limit where  $m_Q \rightarrow \infty$  is appropriate to investigate properties of hadrons containing a single heavy quark. In this limit, the heavy quark behaves as a static color source while the light quarks are moving around. The picture of the heavy-light system is similar to that of an atomic system, where the nucleus remains stationary. The dynamics of an individual atom is independent of the mass and spin orientation of its nucleus. Therefore, if heavy quarks are treated in the same way as atomic nuclei, the dynamics of heavy-light system is therefore independent of their masses and spin orientation. The associated symmetry is  $SU(2)_v$  heavy quark spin symmetry, in which its direct consequences lead to the degeneracy states of the spin 0 and 1 for the heavy mesons and of the spin 1/2 and 3/2 for the heavy baryons.

Generally, the four momentum  $p_Q$  of the heavy quark with mass  $m_Q$  and velocity  $v$  can be expressed as

$$p_Q = m_Q v + k, \quad (3.1)$$

where the off-shell behavior of the heavy quark due to its interaction is described by the residual momentum  $k$ . For heavy hadrons, the typical magnitude of  $k$  is

of the same order as  $\Lambda_{QCD} \sim 200$  MeV. Therefore, the momentum of the heavy quark is mainly contributed by the on-shell component  $m_Q v$  in which  $v^2 = 1$ .

It is convenient to parameterize the heavy quark field  $Q(x)$  in terms of the velocity-dependent, rapidly varying phase, and slowly varying residual fields  $h_v^{(+)}$  and  $h_v^{(-)}$

$$Q(x) = e^{-i(v \cdot x) m_Q} h_v^{(+)}(x) + e^{+i(v \cdot x) m_Q} h_v^{(-)}(x), \quad (3.2)$$

with

$$\begin{aligned} h_v^{(+)} &= e^{+i(v \cdot x) m_Q} P_+ Q(x), \\ h_v^{(-)} &= e^{-i(v \cdot x) m_Q} P_- Q(x). \end{aligned} \quad (3.3)$$

The upper component  $h_v^{(+)}(x)$  annihilates the heavy quark with velocity  $v$  while the anti-heavy quark with velocity  $v$  is created by the lower component  $h_v^{(-)}(x)$ . The projection operators  $P_{\pm}$  can be defined as

$$P_{\pm} = \frac{1 \pm \not{v}}{2}. \quad (3.4)$$

The following identities are satisfied by the projection operator in Eq. (3.4) (Manohar and Wise, 2000),

$$P_{\pm}^2 = P_{\pm},$$

$$P_{\pm} P_{\mp} = 0,$$

$$P_+ + P_- = 1,$$

$$\not{v} h_v^{(+)} = +h_v^{(+)},$$

$$\not{v} h_v^{(-)} = -h_v^{(-)}. \quad (3.5)$$

In the heavy quark limit, the corresponding QCD Lagrangian up to the first order in  $\frac{1}{m_Q}$  is written as,

$$\mathcal{L}_{HQS} = i\bar{h}_v^{(+)} (v \cdot D) h_v^{(+)} + i\bar{h}_v^{(-)} (v \cdot D) h_v^{(-)} + \mathcal{O}\left(\frac{1}{m_Q}\right), \quad (3.6)$$

where  $v \cdot D = v_\mu D^\mu$  denotes the inner product of heavy quark's velocity and the covariant derivative. From the leading order terms in  $\mathcal{L}_{HQS}$ , the fields  $h_v^+$  and  $\bar{h}_v^-$  are decoupled, which implies the decoupling between heavy quark-antiquark at the leading order. This Lagrangian is invariant under the heavy quark spin rotation, i.e., (Georgi, 1990; Neubert, 1994)

$$h_v^\pm \rightarrow e^{-i\mathcal{S} \cdot \theta} h_v^\pm, \quad (3.7)$$

with

$$\mathcal{S}^\mu = \frac{1}{4} \gamma_5 [\not{v}, \gamma^\mu], \mathcal{S}^{\mu\dagger} \gamma_0 = \gamma_0 \mathcal{S}^\mu, [\not{v}, \mathcal{S}^\mu] = 0, \quad (3.8)$$

The generator and the infinitesimal parameters of the  $SU(2)_v$  group are denoted by  $\mathcal{S}^\mu$  and  $\theta_\mu$  respectively. In the rest frame of heavy quark where  $v^\mu = (1, \vec{0})$ , the spatial components of the heavy quark spin generator become

$$\mathcal{S}^k = \frac{1}{4} \gamma_5 [\gamma_0, \gamma^k] = \frac{1}{2} \begin{pmatrix} \sigma^k & 0 \\ 0 & \sigma^k \end{pmatrix} \quad (3.9)$$

### 3.1.2 Building blocks of the heavy quark effective field theory

In the heavy quark limit, the dynamics of heavy-light system is independent of the spin orientation of the heavy quark. As a consequence,  $D$ - and  $D^*$ -mesons are related by a spin flip of the charm quark as for  $\Sigma_c$  and  $\Sigma_c^*$  baryons. Therefore, the following building blocks of heavy quark spin invariant effective Lagrangians are introduced (Cho, 1992; Yan et al., 1992; Wise, 1993; Casalbuoni et al., 1997;

Samart et al., 2016),

$$\begin{aligned}
 H &= \left( \frac{1+\psi}{2} \right) (i\gamma_5 D_+ + \gamma_\mu D_+^\mu), \\
 H_T^\mu &= \frac{1}{\sqrt{3}} (v^\mu + \gamma^\mu) \gamma_5 \left( \frac{1+\psi}{2} \right) \Sigma_{c,+} + \left( \frac{1+\psi}{2} \right) \Sigma_{c,+}^\mu, \\
 H_S &= \frac{1+\psi}{2} \Lambda_{c,+}.
 \end{aligned} \tag{3.10}$$

Under  $SU(2)_v$  symmetry, these building blocks obey the following transformations,

$$\begin{aligned}
 H &\rightarrow e^{-i\mathcal{S}\cdot\theta} H, \\
 H_T^\mu &\rightarrow e^{-i\mathcal{S}\cdot\theta} H_T^\mu, \\
 H_S &\rightarrow H_S,
 \end{aligned} \tag{3.11}$$

In addition, the corresponding  $SU(2)$  isospin transformations for these building blocks are summarized as,

$$\begin{aligned}
 H &\rightarrow e^{-i\alpha\cdot\mathbf{J}} H, \\
 H_T^\mu &\rightarrow e^{-i\alpha\cdot\mathbf{J}} H_T^\mu e^{i\alpha\cdot\mathbf{J}}, \\
 H_T^\mu &\rightarrow e^{-i\alpha\cdot\mathcal{J}} H_T^\mu e^{i\alpha\cdot\mathcal{J}}, \\
 H_S &\rightarrow H_S,
 \end{aligned} \tag{3.12}$$

These transformation laws will be employed to construct heavy quark spin invariant effective Lagrangians for  $D$ -meson, charmed, and light baryons in the next subsection.

### 3.1.3 Heavy quark spin invariant effective Lagrangians

Under  $SU(2)_v$  heavy quark spin transformations in Eq. (3.11) as well as those in Eq. (3.12) and Chapter II, the most general heavy quark spin invariant effective Lagrangian is written as,

$$\begin{aligned}
\mathcal{L}_{HQS} = & c_1 \langle H \gamma_\mu \gamma_\nu \bar{H}_T^\mu v^\nu \gamma_5 N \rangle + c_2 \langle H \gamma_\mu \gamma_\nu \gamma_5 \bar{H}_T^\mu v^\nu N \rangle + c_3 \langle H \gamma_\mu \bar{H}_S v^\mu N \rangle \\
& + c_4 \langle H \gamma_5 \bar{H}_S \gamma_5 N \rangle + c_5 \langle H \sigma_{\mu\nu} \gamma_5 \bar{H}_T^\mu \gamma_5 \Delta^\nu \rangle + c_6 \langle H \sigma_{\mu\nu} \bar{H}_T^\mu \Delta^\nu \rangle \\
& + c_7 \langle H \gamma_5 \bar{H}_T^\mu \gamma_5 \Delta_\mu \rangle + H.c., \tag{3.13}
\end{aligned}$$

where the coupling constants for the heavy quark spin invariant Lagrangians are denoted by  $c_i$  and the symbol  $\langle \dots \rangle$  stands for the trace in the heavy quark spin space. After evaluating the trace in Eq. (3.13), we can rewrite  $\mathcal{L}_{HQS}$  as

$$\begin{aligned}
\mathcal{L}_{HQS} = & c_1 \left( 2D_{+,\mu} \bar{\Sigma}_{c,+}^{(t),\mu} \gamma_5 N + \frac{2}{\sqrt{3}} D_{+,\mu} \bar{\Sigma}_{c,+}^{(t)} \gamma^\mu N \right) \\
& + c_2 \left( -D_{+,\mu} \bar{\Sigma}_{c,+}^{(t),\mu} \gamma_5 N - \sqrt{3} D_+ \bar{\Sigma}_{c,+}^{(t)} i \gamma_5 N + \frac{\sqrt{3}}{12} D_{+,\mu} v_\nu \bar{\Sigma}_{c,+}^{(t)} \sigma^{\mu\nu} N \right) \\
& + c_3 \left( 2D_{+,\mu} \bar{\Lambda}_{c,+} \gamma^\mu N + 2D_{+,\mu} v_\mu \bar{\Lambda}_{c,+} i \sigma^{\mu\nu} N \right) \\
& + c_4 \left( 2i D_+ \bar{\Lambda}_{c,+} \gamma_5 N \right) \\
& - ic_5 \left( -D_{+,\mu} \bar{\Sigma}_{c,+}^{(T)} \gamma_5 \Delta^\mu - 3i D_{+,\mu} v_\nu \bar{\Sigma}_{c,+}^{(T),\mu} \Delta^\nu - 2i D_{+,\mu} \bar{\Sigma}_{c,+}^{(T),\nu} \gamma^\mu \Delta_\nu \right) \\
& + c_6 \left( 2i D_{+,\mu} \bar{\Sigma}_{c,+}^{(T),\mu} \Delta^\nu v_\nu + \frac{2i}{\sqrt{3}} D_{+,\mu} \bar{\Sigma}_{c,+}^{(T)} \gamma^\mu \gamma_5 \Delta^\nu v_\nu \right) \\
& + c_7 \left( -\frac{2i}{\sqrt{3}} D_+ \bar{\Sigma}_{c,+}^{(T)} \Delta^\mu v_\mu + 2i D_+ \bar{\Sigma}_{c,+}^{(T),\mu} \gamma_5 \Delta_\mu \right) + H.c. \tag{3.14}
\end{aligned}$$

### 3.1.4 $1/m_Q$ expansion

According to Eq. (3.2), the  $D$ -meson and charmed baryon fields can be decomposed into such components:

$$\begin{aligned}
D(x) &= e^{-i(v \cdot x) m_c} D_+(x) + e^{+i(v \cdot x) m_c} D_-(x), \\
D^\mu(x) &= e^{-i(v \cdot x) m_c} D_+^\mu(x) + e^{+i(v \cdot x) m_c} D_-^\mu(x), \\
\Lambda_c(x) &= e^{-i(v \cdot x) m_{\Lambda_c}} \Lambda_{c,+}(x) + e^{+i(v \cdot x) m_{\Lambda_c}} \Lambda_{c,-}(x), \\
\Sigma_c(x) &= e^{-i(v \cdot x) m_{\Sigma_c}} \Sigma_{c,+}(x) + e^{+i(v \cdot x) m_{\Sigma_c}} \Sigma_{c,-}(x), \\
\Sigma_c^\mu(x) &= e^{-i(v \cdot x) m_{\Sigma_c^*}} \Sigma_{c,+}^\mu(x) + e^{+i(v \cdot x) m_{\Sigma_c^*}} \Sigma_{c,-}^\mu(x), \tag{3.15}
\end{aligned}$$

with a 4-velocity  $v$  normalized by  $v^2 = 1$ . The mass of charm quark is denoted by  $m_c$  while  $m_{\Lambda_c}$ ,  $m_{\Sigma_c}$ , and  $m_{\Sigma_c^*}$  are those of the isosinglet state  $\Lambda_c$ , the isotriplet states  $\Sigma_c$ , and  $\Sigma_c^*$  respectively. In the heavy quark limit, the mass of  $\Lambda_c$ ,  $\Sigma_c$ , and  $\Sigma_c^*$ , can be replaced by that of charm quark. Therefore, Eq. (3.15) becomes

$$\begin{aligned}
D(x) &= e^{-i(v \cdot x) m_c} D_+(x) + e^{+i(v \cdot x) m_c} D_-(x), \\
D^\mu(x) &= e^{-i(v \cdot x) m_c} D_+^\mu(x) + e^{+i(v \cdot x) m_c} D_-^\mu(x), \\
\Lambda_c(x) &= e^{-i(v \cdot x) m_c} \Lambda_{c,+}(x) + e^{+i(v \cdot x) m_c} \Lambda_{c,-}(x), \\
\Sigma_c(x) &= e^{-i(v \cdot x) m_c} \Sigma_{c,+}(x) + e^{+i(v \cdot x) m_c} \Sigma_{c,-}(x), \\
\Sigma_c^\mu(x) &= e^{-i(v \cdot x) m_c} \Sigma_{c,+}^\mu(x) + e^{+i(v \cdot x) m_c} \Sigma_{c,-}^\mu(x). \tag{3.16}
\end{aligned}$$

According to the properties of  $P_{\pm}$  in Eq. (3.5), the following identities of  $D_+$ ,  $D_{+, \mu}$ ,  $\Sigma_{c,+}$ ,  $\Sigma_{c,+}^{\mu}$ , and  $\Lambda_{c,+}$  are implied,

$$\begin{aligned}
\psi D_+ &= D_+, \\
\psi D_{+, \mu} &= D_{+, \mu}, \\
\psi \Sigma_{c,+} &= \Sigma_{c,+}, \\
\psi \Sigma_{c,+}^{\mu} &= \Sigma_{c,+}^{\mu}, \\
\psi \Lambda_{c,+} &= \Lambda_{c,+}.
\end{aligned} \tag{3.17}$$

In addition, the following transverse relations of  $D^*$ -meson and  $\Sigma_c^*$  baryon are given,

$$\begin{aligned}
v_{\mu} D_+^{\mu} &= 0, \\
v_{\mu} \Sigma_{c,+}^{\mu} &= 0, \\
\gamma_{\mu} \Sigma_{c,+}^{\mu} &= 0.
\end{aligned} \tag{3.18}$$

By using the decompositions of charmed hadron fields in Eq. (3.16) and the properties in Eqs. (3.17)-(3.18), the simplified effective Lagrangian is then written as

$$\begin{aligned}
\mathcal{L} &= g_1 D_+ \bar{\Sigma}_{c,+}^{(t)} \gamma_5 N + g_2 D_+ \bar{\Lambda}_{c,+} \gamma_5 N + g_4 v_{\mu} D_+ \bar{\Sigma}_{c,+}^{(T)} \Delta^{\mu} \\
&+ g_5 D_+ \bar{\Sigma}_{c,+}^{(T), \nu} \gamma_5 \Delta_{\nu} + f_1 D_{+, \mu} \bar{\Sigma}_{c,+}^{(t)} \gamma^{\mu} N + f_2 D_{+, \mu} \bar{\Lambda}_{c,+} \gamma^{\mu} N \\
&+ f_3 D_{+, \mu} \bar{\Sigma}_{c,+}^{(t), \mu} \gamma_5 N + i f_4 D_{+, \mu} \bar{\Sigma}_{c,+}^{(T)} \gamma_5 \Delta^{\mu} + f_5 D_{+, \mu} \bar{\Sigma}_{c,+}^{(T), \nu} \gamma^{\mu} \Delta_{\nu}
\end{aligned}$$



$$\begin{aligned}
& -ih_1 v_\mu D_{+,\nu} \bar{\Sigma}_{c,+}^{(t)} \sigma^{\mu\nu} N - ih_2 v_\mu D_{+,\nu} \bar{\Lambda}_{c,+} \sigma^{\mu\nu} N + ih_3 D_{+,\mu} \bar{\Sigma}_{c,+}^{(t),\mu} \gamma_5 N \\
& + ih_4 (-v_\mu D_{+,\nu} + v_\nu D_{+,\mu}) \bar{\Sigma}_{c,+}^{(T)} \gamma^\mu \gamma_5 \Delta^\nu + \frac{i}{2} h_5 v_\nu D_{+,\mu} \bar{\Sigma}_{c,+}^{(T),\mu} \Delta^\nu + \text{H.c.} \quad (3.19)
\end{aligned}$$

### 3.1.5 Results

By matching the Lagrangians from Eqs. (3.14) and (3.19), following heavy quark sum rules are obtained,

$$\begin{aligned}
g_1 = 3h_1, \quad g_3 = 0, \quad g_4 = \frac{1}{\sqrt{3}} g_5, \quad f_2 = h_2 \\
f_3 = h_3 = \sqrt{3} f_1 - 4\sqrt{3} h_1, \quad f_5 = 2f_4, \quad h_4 = -\frac{1}{2} f_4 + \frac{1}{4\sqrt{3}} h_5. \quad (3.20)
\end{aligned}$$

From heavy quark sum rules, the number of free parameters is reduced down to 7. The corresponding set of free parameters is  $\{g_2, g_5, f_1, f_4, h_1, h_2, h_5\}$ .

## 3.2 Large- $N_c$ picture

### 3.2.1 Introduction

In the low-energy region, QCD is dominated by the non-perturbative dynamics where the strong coupling constant becomes large. As a result, the systematic expansion in terms of the strong coupling constant is no longer applicable. In fact, there exists an additional expansion parameter for QCD which works in both low and high energy domains, the number of color  $N_c$ .

Large  $N_c$  QCD is the  $SU(N_c)$  gauge theory which was introduced in Ref. ('t Hooft, 1974a). In  $SU(N_c)$  group, a color index in the fundamental representation is carried by quarks. On the other hand, a color index in the fundamental conjugate representation is carried by antiquarks. Gluons, which are represented

in the adjoint representation of  $SU(N_c)$ , carry two indices: color and anti-color. Quarks and antiquarks are diagrammatically represented by arrowed lines. For Gluons, they are visualised as two parallel lines whose arrows point in opposite directions, this is called 't Hooft's double line notation (Lebed, 1999).

In the large- $N_c$  limit, i.e.,  $N_c \rightarrow \infty$ , QCD is nontrivial if the following scaling law for the strong coupling constant  $g_s$

$$g_s \propto \frac{1}{\sqrt{N_c}}, \quad (3.21)$$

is held. By studying topology of various diagrams and renormalization group equation, the scaling law in Eq. (3.21) is implied (Lebed, 1999). Relevant  $N_c$  counting rule for a given diagram in the double line notation is determined from the number of closed lines and gauge coupling constants in the original diagram. One can show that the dominant Feynman graphs at the leading order in  $\frac{1}{N_c}$  are planar, which can be drawn in a 2 dimensional plane so that color lines are crossed only at the vertices. In contrast, the non-planar diagrams are suppressed in the large- $N_c$  limit. Here, we summarize the counting rules for the diagrams in large- $N_c$  QCD,

1. Three gluon and quark-gluon vertices scale with the factor  $N_c^{-\frac{1}{2}}$
2. Four gluon vertices scale with the factor  $N_c^{-1}$ .
3. Any closed quark line in a double line representation of a Feynman graph scales with the factor  $N_c$ .
4. Non-planar diagrams are suppressed at least by the factor  $N_c^{-2}$ .

In addition, we summarize the properties of mesons and baryons in the large- $N_c$  limit ('t Hooft, 1974b; Witten, 1979; Dashen et al., 1995; Lutz and Semke, 2011). For mesons, their masses are finite ( $\sim N_c^0$ ) and the vertex with

$n$  mesons scales with a factor of  $N_c^{1-\frac{n}{2}}$ . On the other hand, baryons are heavy ( $\sim N_c$ ), the vertex with two baryon fields and  $n$  meson fields scales with a factor  $N_c^{1-\frac{n}{2}}$ .

### 3.2.2 $1/N_c$ expansion

In the large- $N_c$  limit, matrix elements of the physical baryon states  $|p, \chi\rangle$  can be systematically expanded in terms of those for effective baryon states  $|\chi\rangle$ , which represent the spin and flavor structures of the baryons. We follow the works in Refs. (Luty and March-Russell, 1994; Dashen et al., 1995; Jenkins, 1998; Lutz and Semke, 2011), the expansion in  $\frac{1}{N_c}$  for the baryon matrix elements is represented by

$$\langle p', \chi' | \bar{C}_{i,a}(q) | p, \chi \rangle = \sum_n c_n(p, p') (\chi' | O_{i,a}^{(n)} | \chi), \quad (3.22)$$

where  $\bar{C}_{i,a}(q)$  stands for a correlation operator. The indices  $i$  and  $a$  denote the spatial and isospin indices. The momenta  $p$  and  $p'$  are those of the incoming and outgoing baryons while the momentum of the incoming meson is denoted by  $q$ . The spins of the incoming and outgoing baryons are respectively denoted by  $\chi$  and  $\chi'$ . The effective operator  $O_{i,a}^{(n)}$  are composed by spin, flavor, and spin-flavor operators in  $SU(2)$  flavor symmetry.

The correlation operators in our case are derived by considering the following baryon matrix elements of axial-vector current and vector current operators,

$$\begin{aligned} \langle p', \chi' | A_\mu(x) | p, \chi \rangle &= \frac{\delta}{i\delta a^\mu(x)} \mathcal{F}(p', \chi', p, \chi; v, a), \\ \langle p', \chi' | V_\mu(x) | p, \chi \rangle &= \frac{\delta}{i\delta v^\mu(x)} \mathcal{F}(p', \chi', p, \chi; v, a), \end{aligned} \quad (3.23)$$

with

$$\mathcal{F}(p', \chi', p, \chi; v, a) = \langle p', \chi' | \mathcal{T} : e^{i \int d^4x \{ \mathcal{L}_{EFT}(x) + \mathcal{L}^{aux}(x) \}} : | p, \chi \rangle, \quad (3.24)$$

where  $\mathcal{L}_{EFT}$  denotes the effective Lagrangians in Eqs. (2.17) to (2.18). The couplings between  $D$  meson fields and the classical sources ( $a^\mu$  and  $v^\mu$ ) are described by the auxiliary Lagrangian,

$$\begin{aligned} \mathcal{L}^{aux}(x) &= \mathcal{L}_A^{aux}(x) + \mathcal{L}_V^{aux}(x), \\ &= \frac{f_A}{m_A} \left( a^\mu \partial_\mu \bar{D} + \partial_\mu \bar{a}^\mu \right) + f_V \left( v^\mu \bar{D}_\mu + D_\mu \bar{v}^\mu \right), \end{aligned} \quad (3.25)$$

with

$$\bar{a}^\mu = a^{\mu\dagger} \text{ and } \bar{v}^\mu = v^{\mu\dagger}. \quad (3.26)$$

The parameters  $f_A$  and  $f_V$  denote the coupling constants while the mass of the classical source  $a^\mu$  is written as  $m_A$ . In this auxiliary Lagrangian, the external sources  $a^\mu$  and  $v^\mu$  transform as axial-vector and vector respectively. The operators  $C_\mu^A(q)$  and  $C_\mu^V(q)$  are obtained from the following transformations

$$\begin{aligned} C_\mu^A(q) &= i \int d^4x e^{-iq \cdot x} A_\mu(q), \\ C_\mu^V(q) &= i \int d^4x e^{-iq \cdot x} V_\mu(q). \end{aligned} \quad (3.27)$$

It is convenient to introduce the operator

$$\bar{C}_{\mu,a}^X(q) = \frac{q^2 - m_X^2}{f_X} C_{\mu,a}^X(q), \quad (3.28)$$

with  $X = V, A$  and  $m_A$  and  $m_V$  are the masses of the pseudoscalar and vector  $D$  mesons. In the non-relativistic limit, the spatial components of the operator  $\bar{C}_{\mu,a}^X(q)$  are kept. Therefore, the Lorentz indices are replaced by the spatial indices,

as we have already shown in Eq. (3.22).

The following effective operators in  $SU(2)$  flavor symmetry with their  $N_c$  scaling laws are introduced to construct the operator  $O_{i,a}^{(n)}$  which enters Eq. (3.22) (Dashen et al., 1995),

$$J^i = \frac{1}{2} q_{A\mu}^\dagger \sigma_{\mu\nu}^i q_{A\nu} \sim 1/N_c, \quad (3.29)$$

$$I^a = \frac{1}{2} q_{A\mu}^\dagger \tau_{AB}^a q_{B\mu} \sim 1/N_c, \quad (3.30)$$

$$G^{ia} = \frac{1}{4} q_{A\mu}^\dagger \sigma_{\mu\nu}^i \tau_{AB}^a q_{B\nu} \sim N_c^0, \quad (3.31)$$

$$Y^{iA} = \frac{1}{2} C_\mu^\dagger \sigma_{\mu\nu}^i q_{A\nu} \sim \sqrt{N_c}, \quad (3.32)$$

$$t^A = C_\mu^\dagger q_{A\mu} \sim \sqrt{N_c}, \quad (3.33)$$

$$N_h = C_\mu^\dagger C_\mu \sim N_c^0, \quad (3.34)$$

$$J_h^i = \frac{1}{2} C_\mu^\dagger \sigma_{\mu\nu}^i C_\nu \sim 1/N_c. \quad (3.35)$$

Therefore, the corresponding effective axial-vector and vector operators (at the leading order of  $N_c$ ) are written as,

$$A^{i,E} = c_1^A q^i k^j Y^{jE} + c_2^A q^i q^j Y^{jE} + c_3^A q^i q^j J^j t^E, \quad (3.36)$$

and

$$V^{i,E} = c_1^V q^i t^E + c_2^V \epsilon^{ijk} q^j Y^{kE} + c_3^V k^i t^E + c_4^V q^j J^j Y^{iE}, \quad (3.37)$$

where  $p' + p = k \sim N_c^0$  and  $p' - p = q \sim N_c^0$ . According to the  $N_c$  scalings of the effective operators, the scaling laws for the constants  $c_i$  are given by  $c_1^A, c_2^A, c_1^V, c_2^V, c_3^V \sim \sqrt{N_c}$  and  $c_3^A, c_4^V \sim N_c^{-1/2}$ .

### 3.2.3 Results

Here, we refer to the Ph.D. thesis of T. Suyuporn. By performing  $\frac{1}{N_c}$  expansion to the baryon matrix element of correlation operators in Eq. (3.28) and effective operators in Eqs. (3.36) and (3.37), the following sum rules are derived,

$$\begin{aligned}
 g_2 &= -\frac{3}{2\sqrt{3}}g_1, & g_3 &= 0, & g_5 &= -\frac{3\sqrt{3}}{2}g_1, & f_2 &= \sqrt{3}f_1, \\
 f_5 &= -\frac{3\sqrt{3}}{2}f_1, & h_1 &= \frac{\sqrt{3}}{2}h_2, & h_3 &= h_4 = 0, & h_5 &= -\sqrt{3}f_1.
 \end{aligned} \tag{3.38}$$

These large- $N_c$  constraints reduces the number of free parameters down to 6, the corresponding set of free parameters is  $\{g_1, g_4, f_1, f_3, f_4, h_2\}$ .

### 3.3 Combining heavy quark and large- $N_c$ constraints

If the heavy quark and large- $N_c$  constraints in Eqs. (3.20) and (3.38) are combined, the combining heavy quark and large- $N_c$  constraints are then given as

$$\begin{aligned}
 g_1 &= -\frac{2}{3}g_4, & g_2 &= -\frac{3\sqrt{3}}{2}h_1, & g_3 &= 0, & f_1 &= 4h_1, \\
 f_2 &= -h_5 = \frac{2}{\sqrt{3}}h_1, & f_3 &= h_3 = h_4 = 0, & f_4 &= \frac{1}{2\sqrt{3}}h_5.
 \end{aligned} \tag{3.39}$$

where the set of free parameters from combining heavy quark and large- $N_c$  constraints is  $\{g_5, f_5, h_1, h_2, h_5\}$ .

# CHAPTER IV

## ESTIMATION OF COUPLING CONSTANTS

### IN QUARK MODEL

In this chapter, we estimate the coupling constants for the effective Lagrangians of  $D$ -meson, charmed, and light baryons through various decay processes of  $\Lambda_c$  and  $\Sigma_c$  baryons. First, we calculate the decay widths for the following processes:  $\Lambda_c \rightarrow D^*N$ ,  $\Lambda_c \rightarrow DN$ ,  $\Sigma_c \rightarrow DN$ ,  $\Sigma_c \rightarrow D\Delta$ , and  $\Sigma_c \rightarrow D^*\Delta$ , using the effective Lagrangian method and quark model picture with the  ${}^3P_0$  model. Next, we use coupling constants for  $D^*\Lambda_c N$  interaction from various literature to fix the strength parameter  $\lambda$  for the  ${}^3P_0$  model in the decay process  $\Lambda_c \rightarrow D^*N$ . Then, we estimate the coupling constants for the effective Lagrangians of  $D\Lambda_c N$ ,  $D\Sigma_c N$ ,  $D\Sigma_c \Delta$ , and  $D^*\Sigma_c \Delta$  interactions in the decay channels  $\Lambda_c \rightarrow DN$ ,  $\Sigma_c \rightarrow DN$ ,  $\Sigma_c \rightarrow D\Delta$ , and  $\Sigma_c \rightarrow D^*\Delta$ , respectively. Finally, we use the combining heavy-quark and large- $N_c$  sum rules derived in Chapter III to calculate the coupling constants for  $D\Sigma_c N$ ,  $D^*\Sigma_c N$ , and  $D^*\Sigma_c^* \Delta$  interactions.

#### 4.1 Feynman amplitudes

In this section, we calculate decay widths of charmed baryons in effective Lagrangian method. The decay of an initial charmed baryon  $B_c$  into an outgoing light baryon  $B$  and a charmed meson  $\phi_c$  is displayed by the diagram in Figure 4.1.

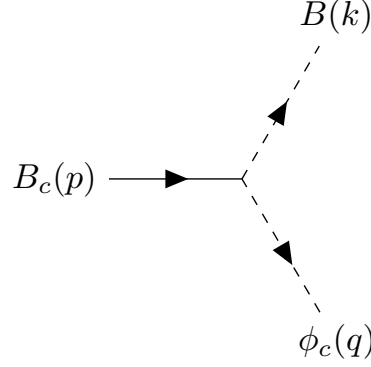


**Figure 4.1** Feynman diagram for the decay process  $B_c(p, s) \rightarrow B(k, s') \phi_c(q, s'')$ .

Here, the momentum of the initial charmed baryon ( $\Lambda_c(2286)$  or  $\Sigma_c(2455)$ ) is denoted by  $p$ , while  $k$  and  $q$  are those of the outgoing light baryon ( $N(939)$  or  $\Delta(1232)$ ) and charmed meson ( $D(1868)$  or  $D^*(2009)$ ) respectively. The spin projections of the initial charmed baryon, outgoing light baryon and charmed meson are respectively denoted by  $s$ ,  $s'$ , and  $s''$ .

To compare our results with those in Refs. (Khodjamirian et al., 2012; Azizi et al., 2014; Azizi et al., 2015b), we introduce the following additional Lagrangians:

$$\mathcal{L}_{D\Sigma_c N}^{(P)} = g'_1 D \bar{\Sigma}_c^{(t)} i \gamma_5 N + H.c., \quad (4.1)$$

$$\mathcal{L}_{D\Lambda_c N}^{(P)} = g'_2 D \bar{\Lambda}_c i \gamma_5 N + H.c., \quad (4.2)$$

where  $g'_1$  and  $g'_2$  are pseudoscalar coupling constants for the corresponding interaction vertices. By employing Lagrangians in Eqs. (2.17) to (2.18) and Eqs. (4.1) to (4.2), Feynman amplitudes for the decay processes  $\Sigma_c \rightarrow DN$ ,  $\Lambda_c \rightarrow DN$ ,  $\Sigma_c \rightarrow D\Delta$ ,  $\Lambda_c \rightarrow D^*N$ , and  $\Sigma_c \rightarrow D^*\Delta$  are written as

$$\mathcal{M}_{\Sigma_c \rightarrow DN}^{(P)} = -g'_1 \bar{u}_N(k, s') \gamma_5 u_{\Sigma_c}(p, s), \quad (4.3)$$

$$\mathcal{M}_{\Lambda_c \rightarrow DN}^{(A)} = \frac{g_2}{m_D} \bar{u}_N(k, s') \not{q} \gamma_5 u_{\Lambda_c}(p, s), \quad (4.4)$$



$$\mathcal{M}_{\Lambda_c \rightarrow DN}^{(P)} = -g_2' \bar{u}_N(k, s') \gamma_5 u_{\Lambda_c}(p, s), \quad (4.5)$$

$$\mathcal{M}_{\Sigma_c \rightarrow D\Delta} = -\frac{g_4}{m_D} q_\mu \bar{u}_\Delta^\mu(k, s') u_{\Sigma_c}(p, s), \quad (4.6)$$

$$\mathcal{M}_{\Lambda_c \rightarrow D^*N} = i f_2 \bar{u}_N(k, s') \Gamma^\mu u_{\Lambda_c}(p, s) \epsilon_\mu^*(q, s''), \quad (4.7)$$

$$\mathcal{M}_{\Sigma_c \rightarrow D^*\Delta} = i f_4 \bar{u}_\Delta^\mu(k, s') \gamma_5 u_{\Sigma_c}(p, s) \epsilon_\mu^*(q, s''), \quad (4.8)$$

where

$$\Gamma^\mu = \left[ \gamma^\mu + \frac{i}{m_D} \left( \frac{h_2}{f_2} \right) \sigma^{\mu\nu} q_\nu \right]. \quad (4.9)$$

The decay width of the initial charmed baryon  $B_c$  is then computed from

$$\Gamma_{\text{EFT}} = \frac{1}{32\pi^2} \frac{|\vec{q}|}{m_{B_c}} \int \langle |\mathcal{M}|^2 \rangle d\Omega, \quad (4.10)$$

where

$$\langle |\mathcal{M}|^2 \rangle = \begin{cases} \frac{1}{2} \sum_{s'} |\mathcal{M}|^2 & \text{if } \phi_c = D, \\ \frac{1}{2} \sum_{s', s''} |\mathcal{M}|^2 & \text{if } \phi_c = D^*. \end{cases} \quad (4.11)$$

The mass of the initial charmed baryon and the magnitude of outgoing 3-momentum in the center of mass frame of the initial charmed baryon are denoted by  $m_{B_c}$  and  $|\vec{q}|$ .

By expanding the decay width with respect to the outgoing 3-momentum  $q$  near the threshold, the following expressions for the decay widths are obtained

$$\Gamma_{\Sigma_c \rightarrow DN}^{(P)} = \frac{g_1'^2}{8\pi m_N m_{\Sigma_c}} q^3, \quad (4.12)$$

$$\Gamma_{\Lambda_c \rightarrow DN}^{(A)} = \frac{g_2^2 (m_D + 2m_N)^2}{8\pi m_D^2 m_N m_{\Lambda_c}} q^3, \quad (4.13)$$

$$\Gamma_{\Lambda_c \rightarrow DN}^{(P)} = \frac{g_2'^2}{8\pi m_N m_{\Lambda_c}} q^3, \quad (4.14)$$

$$\Gamma_{\Sigma_c \rightarrow D\Delta} = \frac{g_4^2 (m_D + m_\Delta)^2}{3\pi m_D^2 m_\Delta m_{\Sigma_c}} q^3, \quad (4.15)$$

$$\Gamma_{\Lambda_c \rightarrow D^*N} = \frac{\mathcal{A}}{8\pi m_D^2 m_{D^*}^2 m_N m_{\Lambda_c}} q^3, \quad (4.16)$$

$$\Gamma_{\Sigma_c \rightarrow D^*\Delta} = \frac{f_4^2}{4\pi m_\Delta m_{\Sigma_c}} q^3, \quad (4.17)$$

where

$$\begin{aligned} \mathcal{A} = & f_2^2 \left( 3m_{D^*}^2 m_D^2 + 4m_{D^*} m_N m_D^2 + 4m_N^2 m_D^2 \right) - 6f_2 h_2 \left( m_{D^*}^3 m_D + 2m_{D^*}^2 m_N m_D \right) \\ & + h_2^2 \left( 3m_{D^*}^4 + 8m_{D^*}^3 m_N + 8m_N^2 m_{D^*}^2 \right). \end{aligned} \quad (4.18)$$

We note that the decay widths in Eqs. (4.12) to (4.17) are held for real and imaginary outgoing momenta.

## 4.2 Quark model

In this section, decay widths of the same decay processes as in Section 4.1 are calculated in a quark model picture with the  ${}^3P_0$  model. The corresponding diagram is displayed in Figure 4.2. Here, the decay process  $B_c \rightarrow B\phi_c$  may arise from the  $qq$  and  $c$  of the initial state  $B_c$  which are directly dressed by two additional quark-antiquark pair pumped out of the vacuum to form  $B$  and  $\phi_c$  in the final state. The transition amplitude derived in the  ${}^3P_0$  model is written as

$$T = \langle B\phi_c | V_{q\bar{q}} | B_c \rangle, \quad (4.19)$$

where  $V_{q\bar{q}}$  corresponds to the effective quark-antiquark vertex. The  ${}^3P_0$  model defines the quantum states of quark-antiquark pair that are destroyed into or created from vacuum ( ${}^3P_0$ , isospin  $I = 0$ , and color singlet). The effective quark-antiquark vertex in the  ${}^3P_0$  model is defined according to Refs. (Yan et al., 2005;

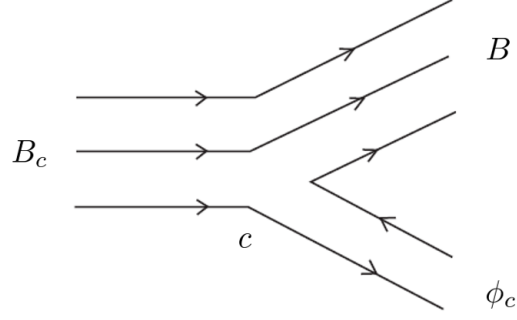


**Figure 4.2** Schematic diagram for the decay process  $B_c \rightarrow B\phi_c$  in  ${}^3P_0$  quark model. The bottom quark line is that of charm quark while the rest are those of  $u$  and  $d$  quarks.

Kittimanapun et al., 2009):

$$\begin{aligned}
 V_{q\bar{q}}^{ij} &= \lambda \vec{\sigma}_{ij} \cdot (\vec{p}_i - \vec{p}_j) \hat{F}_{ij} \hat{C}_{ij} \delta(\vec{p}_i + \vec{p}_j) \\
 &= \lambda \sum_{\mu} \sqrt{\frac{4\pi}{3}} (-1)^{\mu} \sigma_{ij}^{\mu} Y_{1\mu}(\vec{p}_i - \vec{p}_j) \hat{F}_{ij} \hat{C}_{ij} \delta(\vec{p}_i + \vec{p}_j)
 \end{aligned} \tag{4.20}$$

where the parameter  $\lambda$  denotes the effective coupling strength of the  ${}^3P_0$  vertex. The spin operator that creates (or annihilates) the spin-1  $q\bar{q}$  pair is denoted by  $\sigma_{ij}^{\mu}$  and  $Y_{1\mu}(\vec{p})$  corresponds to the spherical harmonics in the momentum space. The flavor and color unit operators are denoted by  $\hat{F}_{ij}$  and  $\hat{C}_{ij}$ .

In this work, the baryon and meson spatial wave functions are approximated with the Gaussian form Ref. (Faessler et al., 2010). The flavor and spin parts are constructed in the framework of the  $SU(2)$  flavor and  $SU(2)$  spin symmetries. The transition amplitude is obtained as

$$T = \lambda \sqrt{\frac{4\pi}{3}} C_i f e^{-Qq^2} C(S_i s_i; 1\mu; S_f, s_i + \mu), \tag{4.21}$$

with

$$\begin{aligned}
f &= -\frac{6\sqrt{3}a^3b^{3/2}(b^2m_r + 2a^2(1 + m_r))|\bar{q}|}{(3a^2 + b^2)^{5/2}(1 + m_r)\pi^{3/4}}, \\
Q &= \frac{a^2(3a^2(1 + m_r)^2 + b^2(5 - 2m_r + 2m_r^2))}{6(3a^2 + b^2)(1 + m_r)^2}, \\
C_i &= \frac{2}{\sqrt{3}} \left( \frac{1}{\sqrt{2}} \right)^{\delta_{S', \frac{1}{2}}} \\
&\quad \frac{\sqrt{(2S' + 1)(2S'' + 1)(2S_i + 1)(3)}}{\sqrt{(2T' + 1)(2T'' + 1)(2T_i + 1)(1)}} \\
&\quad \left\{ \begin{matrix} T_i & (6) & S' \\ (8) & (7) & S'' \\ S_i & 1 & S_f \end{matrix} \right\} \left\{ \begin{matrix} T_i & (6) & T' \\ 0 & (7) & T'' \\ T_i & 0 & T_f \end{matrix} \right\}, \tag{4.22}
\end{aligned}$$

where  $(S_i, T_i)$ ,  $(S', T')$ , and  $(S'', T'')$  denote the spin-isospin of the states  $B_c$ ,  $B$ , and  $\phi_c$ , respectively. The spin  $S_f$  and isospin  $T_f$  are defined by  $S_f = S' \otimes S''$  and  $T_f = T' \otimes T''$ . The spin projections of the  $q\bar{q}$  pair in the  ${}^3P_0$  model and the initial charmed baryon  $B_c$  are denoted by  $\mu$  and  $s_i$ .  $C$  is the Clebsch-Gordan coefficient. The parameter  $m_r \equiv m_q/m_Q$  is the ratio between the light quark mass  $m_q$  and heavy quark mass  $m_Q$ . The value of  $m_r$  in this study is 300/1270.  $\delta$  is the Kronecker delta and the brackets  $\{ \}$  in  $C_i$  are the 9-j symbols. The flavor-spin-color factors  $C_i$  for the decay processes in this study are summarized in Table 4.1. The baryon and meson length parameters  $a$  and  $b$  are respectively  $3.0 \text{ GeV}^{-1}$  and  $2.28 \text{ GeV}^{-1}$  (Isgur and Karl, 1979; Sreethawong et al., 2015; Dover et al., 1992; Muhm et al., 1996; Limphirat et al., 2014).

**Table 4.1** The flavor-spin-color factors  $C_i$  corresponding to the decay processes  $B_c \rightarrow B\phi_c$ .

Processes	$C_i$	
	$S_f = 1/2$	$S_f = 3/2$
$\Lambda_c(2286) \rightarrow ND$	$\frac{1}{\sqrt{2}}$	
$\Lambda_c(2286) \rightarrow ND^*$	$-\frac{1}{\sqrt{6}}$	$\sqrt{\frac{2}{3}}$
$\Sigma_c(2455) \rightarrow ND$	$\frac{1}{3\sqrt{6}}$	
$\Sigma_c(2455) \rightarrow \Delta D$	$-\frac{2}{3}\sqrt{\frac{2}{3}}$	
$\Sigma_c(2455) \rightarrow \Delta D^*$	$\frac{4}{9}$	$\frac{2\sqrt{10}}{9}$

The decay width of the charmed baryon  $B_c$  is calculated from

$$\Gamma_{\text{QM}} = \frac{2\pi E' E'' |\vec{q}|}{m_{B_c} (2S_i + 1)} \sum_{s_i, \mu, S_f} |T|^2, \quad (4.23)$$

where  $E'$  and  $E''$  denote energies of the outgoing light baryon  $B$  and charmed meson  $\phi_c$  while  $|\vec{q}|$  and  $m_{B_c}$  are similar to those in Eq. (4.10).

### 4.3 Results

In this section, we estimate the coupling constants from the decay widths calculated in Sections 4.1 and 4.2. Considering that the decay width formulas in Eqs. (4.12) to (4.17) and Eq. (4.23) hold for both the real and imaginary values of the outgoing momentum  $q$ , one may estimate the coupling constants by applying the near threshold off-shell decay processes of  $\Lambda_c$  and  $\Sigma_c$  baryons under consideration. In the low  $q$  region, one requires

$$\Gamma_{\text{EFT}} = \Gamma_{\text{QM}}. \quad (4.24)$$

The coupling constants determined from Eq. (4.24) are those at  $q^2 = 0$ . For comparison, we employ as inputs five different sets of the coupling constants  $f_{D^*\Lambda_c N}$  and  $h_{D^*\Lambda_c N}$  from Refs. (Kim et al., 2015; Sangkhakrit et al., 2022; Khodjamirian

et al., 2012; Titov and Kampf, 2008; Azizi et al., 2015a) for the decay process  $\Lambda_c \rightarrow D^*N$ . From Eq. (4.24), we fix the  ${}^3P_0$  strength parameter  $\lambda$  in Eq. (4.21) for each input set and then use its value to estimate the coupling constants  $g_{D\Lambda_c N}^{(P)}$ ,  $g_{D\Lambda_c N}^{(A)}$ ,  $g_{D\Sigma_c\Delta}$ ,  $f_{D^*\Sigma_c\Delta}$ , and  $g_{D\Sigma_c N}^{(P)}$  of the effective Lagrangians. Then, these results are used to determine the coupling constants  $g_{D\Sigma_c N}^{(A)}$ ,  $f_{D^*\Sigma_c N}$ ,  $h_{D^*\Sigma_c N}$ , and  $h_{D^*\Sigma_c^*\Delta}$  from the combining heavy quark and large- $N_c$  sum rules in Eq. (3.39). In our case, we assume that all coupling constants are positive and they are displayed in Table 4.2.

**Table 4.2** Coupling constants of  $D$ -meson, charmed, and light baryons from our estimation. The numbers in the brackets denote the magnitudes of the original coupling constants used in the cited literature ([a] (Kim et al., 2015), [b] (Sangkhakrit et al., 2022), [c] (Khodjamirian et al., 2012), [d] (Titov and Kampf, 2008), [e] (Azizi et al., 2015a), [f] (Azizi et al., 2014), [g] (Fontoura et al., 2017), [h] (Azizi et al., 2015b), [i] (Yu et al., 2019)), if available.

Input ( $f_{D^*\Lambda_c N}, h_{D^*\Lambda_c N}$ )	Results								
	$g_{D\Lambda_c N}^{(P)}$	$g_{D\Lambda_c N}^{(A)}$	$g_{D\Sigma_c\Delta}$	$f_{D^*\Sigma_c\Delta}$	$g_{D\Sigma_c N}^{(P)}$	$g_{D\Sigma_c N}^{(A)}$	$f_{D^*\Sigma_c N}$	$h_{D^*\Sigma_c N}$	$h_{D^*\Sigma_c^*\Delta}$
(-4.26, -12.4) [a]	17.57	15.12 (13.4 [a])	9.28	26.05	3.38	11.22	13.5 (2.46 [a])	6.12 (1.31 [a])	3.89
(-5.11, -10.4) [b]	16.65	14.33 (13.5 [b])	8.79	24.68	3.2	10.63 (2.5 [b])	12.7 (4.182 [b])	5.8 (2.87 [b])	3.69
(5.8, 3.6) [c]	11.1 (10.7 [c])	9.55	5.86	16.45	2.13 (1.3 [c])	7.08	8.52 (1.0 [c])	3.86 (2.1 [c])	2.46
(-5.18, -14.4) [d]	20.66	17.78	10.9	30.62	3.98	13.18	15.87 (3.29 [d])	7.2 (2.99 [d])	4.58
(2.21, 7.26) [e]	9.86 (0.91 [f])	8.49 (15.25 [g]) (7.28 [f])	5.21	14.62	1.89 (3.78 [h])	6.3	7.58 (11.14 [e]) (13.7 [i])	3.44 (5.40 [e]) (15.3 [i])	2.19

Here, we have used  $g_{D\Sigma_c N}^{(P)} = g'_1$ ,  $g_{D\Lambda_c N}^{(P)} = g'_2$ ,  $g_{D\Sigma_c\Delta} = g_4$ , and  $f_{D^*\Sigma_c\Delta} = f_4$ . The coupling constants  $g_{D\Lambda_c N}^{(A)}$ ,  $f_{D^*\Lambda_c N}$ , and  $h_{D^*\Lambda_c N}$  are obtained by rescaling the coupling constants  $g_2$ ,  $f_2$ , and  $h_2$  to those in Refs. (Kim et al., 2015; Sangkhakrit

et al., 2022; Titov and Kampfer, 2008). Note that the expressions for the coupling constants resulted from Eq. (4.24) are independent of the corresponding initial masses.

From our study, we have found that the magnitudes of the coupling constants are of the same orders as those in the cited literatures. As the original values of  $g_{D\Sigma_c\Delta}$ ,  $f_{D^*\Sigma_c\Delta}$ , and  $h_{D^*\Sigma_c^*\Delta}$  are not presented anywhere, we only display the results from our estimation.



# CHAPTER V

## PRODUCTIONS OF STRANGE AND CHARMED BARYONS IN EFFECTIVE LAGRANGIAN AND REGGE APPROACHES

The effective Lagrangian method is a well-established tool for describing the low-energy behavior of experimental production rates. However, this approach encounters challenges when applied to the high-energy regime due to the violation of unitarity, leading to incorrect predictions. To address this issue, we propose a second model based on the Regge approach, which is capable of reproducing both the forward and backward peaks observed in high-energy scatterings. The fundamental principle of unitarity is preserved in this model, ensuring the correct asymptotic behavior of production rates in the high-energy region.

In this chapter, we first present an overview of the Regge approach, which is based on the exchange of particles with non-zero spin and is particularly suited for the high-energy regime. We then apply the effective Lagrangian method and the Regge model to study various strangeness productions, and determine the model parameters through a rigorous fitting procedure to experimental data. The scaling parameters for Regge amplitudes is evaluated using Kaidalov's Quark-Gluon String Model (QGSM) (Kaidalov and Volkovitsky, 1994), which is a well-established theoretical framework for describing high-energy hadronic interactions.

Finally, we use the established models to predict the production rates of various charmed baryons. Specifically, we replace the kinematical parameters for



strange hadrons with those for charm hadrons to obtain the corresponding cross-sections. The predicted results from both the effective Lagrangian and Regge models are compared and analyzed in detail to gain insights into the underlying mechanisms of these productions.

## 5.1 Introduction

In most scattering processes, there exists a tendency for a strong forward peak, which becomes obvious in the high-energy region. The magnitude of the cross section for a particular process depends on whether a  $t$ -channel process is included or not. These observations are also held for the presence of a backward peak and the inclusion of a  $u$ -channel process. For these reasons, there is a correlation between the presence of a forward (backward) peak in  $s$ -channel processes and the exchange of particles or resonances in the  $t$ -channel ( $u$ -channel) (Collins, 1971; Donnachie et al., 2004).

Regge theory is applicable to reproduce the forward angle behavior in the region with large  $s$  and small  $t$ . It is also applicable for the backward angle behavior in the one with large  $s$  and small  $u$ . To derive the transition amplitude in Regge representation, we first consider the partial-wave expansion of the amplitude  $A(s, t)$  in the physical region of the  $t$ -channel ( $s < 0$  and  $t > 4m^2$ )

$$A(s, t) = 16\pi \sum_{l=0}^{\infty} (2l+1) A_l(t) P_l(z_t), \quad (5.1)$$

with

$$z_t = \cos\theta_t = 1 + \frac{2s}{t - 4m^2}, \quad (5.2)$$

in the equal-mass case. At large  $s$ , the series expansion in Eq. (5.1) diverges because  $P_l(z_t) \sim s^l$ . If we consider the contribution of only one partial wave, this divergence problem is therefore avoided. However, the energy dependence of

a corresponding cross section contradicts with that of an observed experimental data. Instead of a single particle exchange, ground states and the series of excited states in the  $t$ -channel exchange process must be combined in such a way that the observed energy dependence is reproduced. For this reason, we shall terminate the summation in Eq. (5.1) at a certain maximum value of angular momentum  $l_{max}$ . Then, we rewrite it as a contour integral in the complex angular momentum plane and perform the analytical continuation to the physical region of  $s$ -channel ( $s > 0$  and  $t < 4m^2$ ).

To do this, we introduce the amplitudes with even-signature  $A_l^+(t)$  and odd-signature  $A_l^-(t)$  as

$$A_l(t) = \begin{cases} A_l^+(t), & l \text{ even,} \\ A_l^-(t), & l \text{ odd.} \end{cases} \quad (5.3)$$

Then, the partial wave expansion in Eq. (5.1) can be rewritten in terms of these signated amplitudes:

$$A^\pm(s, t) = 8\pi \sum_{l=0}^{\infty} (2l+1) A_l^\pm(t) (P_l(z_t) \pm P_l(-z_t)). \quad (5.4)$$

By using Cauchy's theorem, one can rewrite the partial wave amplitude into the contour integral of the complex angular momentum  $l$  as

$$A^\pm(s, t) = \int_C dl (2l+1) A^\pm(l, t) \frac{P_l(z_t) \pm P_l(-z_t)}{\sin \pi l}, \quad (5.5)$$

where the real axis is surrounded by the contour  $C$  from 0 to  $\infty$ . The corresponding poles are located at the points  $l = 0, 1, 2, \dots$ . We finally obtain the Regge representation of the transition amplitudes  $A^\pm(s, t)$ :

$$A^\pm(s, t) \sim \sum_j \beta_j^\pm(t) \Gamma(-\alpha_j^\pm(t)) \xi_\alpha^\pm \left( \frac{s}{s_0} \right)^{\alpha_j^\pm(t)}, \quad (5.6)$$

where the positions of the poles and their residues are identified by  $\alpha_j^\pm(t)$  and  $\beta_j^\pm(t)$ , respectively. The signature factor  $\xi_\alpha^\pm$  is written as

$$\xi_\alpha^\pm = 1 \pm e^{-i\pi\alpha_j^\pm(t)}, \quad (5.7)$$

and the scale parameter is denoted by  $s_0$ . The direct observation from Eq. (5.6) is that, the poles of the transition amplitude in the complex angular momentum space are related to bound or resonance states. These poles are also known as Regge poles or Reggeons. The exchanges of families of hadrons, which contain the same quantum numbers, are described by Regge trajectories  $\alpha(t)$ . The spin  $J$  and mass  $m$  of the corresponding hadron are related by  $\alpha(m^2) = J$ .

## 5.2 Unitarity

In the case where only one partial wave is contributed, the transition amplitude is therefore written as  $A(s, t) \sim g(t)s^J$ . By doing this, the divergence of the partial wave expansion is temporarily avoided. However, the consistency between this transition amplitude and the unitarity is demanded. Otherwise, one may not be able to correctly reproduce the high-energy behavior of the observed cross sections. To start with, the total cross section and the forward elastic scattering amplitude of the reaction  $A + B \rightarrow A + B$  are related by the following optical theorem

$$\sigma_{AB}^{total} = \frac{1}{2|\mathbf{p}_1|\sqrt{s}} \text{Im} A(s, t = 0), \quad (5.8)$$

where  $|\mathbf{p}_1|$  denotes the magnitude of the initial three-momentum in the center of mass frame while  $A(s, t)$  is the corresponding elastic scattering amplitude. In the region where  $s$  is large, the total cross section behaves as  $\sigma^{total} \sim s^{J-1}$ . When particles with higher spins are exchanged, i.e.,  $J \geq 2$ , the unitarity is violated.

From the Froissart bound, the behavior of  $\sigma^{total}$  in this region is

$$\sigma^{total} \leq \text{constant} \times \left( \log \left( \frac{s}{s_0} \right) \right)^2. \quad (5.9)$$

Therefore, we are demanded to include all possible hadrons which belong to the same trajectory such that the unitarity is conserved.

According to the consistency between Regge model and unitarity, the high-energy behavior of differential cross sections is therefore well reproduced, especially in the forward angle region. As  $s \rightarrow \infty$ , the following asymptotic behavior of differential cross sections

$$\frac{d\sigma}{dt} (s \rightarrow \infty, t \rightarrow 0) \propto s^{2(\alpha(t)-1)}, \quad (5.10)$$

is given.

Since Regge model is mostly applicable in the diffractive region, the behavior of the production rates near the threshold may not be reproduced well. On the other hand, effective Lagrangian approach is applicable at reproducing low-energy behavior of various cross sections. Therefore, it is appropriate to investigate production rates of strange and charmed baryons within these two approaches. By doing this, the low- and high-energy behaviors of the production rates are provided at the same time. First, various strange and charm production rates in  $p\bar{p}$  collisions will be studied in effective Lagrangian method. Then, the same reaction processes will be discussed in Regge model.

## 5.3 Effective Lagrangian approach

### 5.3.1 Feynman amplitudes

In this section, strangeness and charm productions will be studied in effective Lagrangian approach. First, we consider strangeness productions from proton-antiproton interactions. The corresponding tree-level diagram is displayed in Figure 5.1, where  $Y$  and  $\bar{Y}'$  denote a produced hyperon ( $\Lambda^0$  or  $\Sigma^0$ ) and its antiparticle ( $\bar{\Lambda}^0$  or  $\bar{\Sigma}^0$ ). An exchanged strange meson ( $K^+$  or  $K^{*+}$ ) is denoted by  $\phi$ . The momenta of the incoming proton and antiproton are denoted by  $p_1$  and  $p_2$  while  $q$ ,  $p_3$ , and  $p_4$  are those of the exchanged strange meson, outgoing hyperon, and antihyperon, respectively. Here, we assume that cross sections for such processes are dominated by  $t$ -channel exchanges, this assumption is reasonable for the scattering at energy that are sufficient above the threshold. The effective

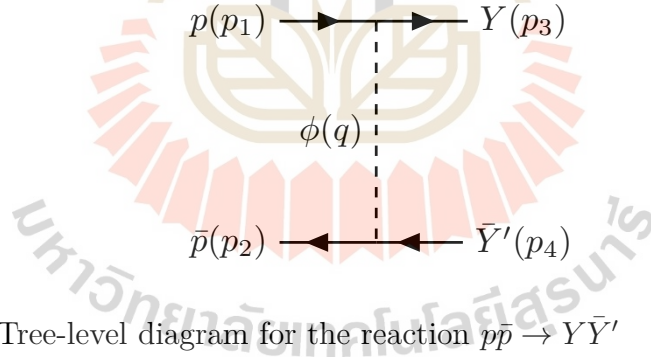


**Figure 5.1** Tree-level diagram for the reaction  $p\bar{p} \rightarrow Y\bar{Y}'$

Lagrangians for  $KNY$  and  $K^*NY$  vertices are (Kim et al., 2015)

$$\mathcal{L}_{KNY} = \frac{g_{KNY}}{m_N + m_Y} \bar{N} \gamma^\mu \gamma_5 Y \partial_\mu K + \text{H.c.}, \quad (5.11)$$

$$\mathcal{L}_{K^*NY} = -g_{K^*NY} \bar{N} \left[ \gamma^\mu Y - \frac{\kappa_{K^*NY}}{m_N + m_Y} \sigma^{\mu\nu} Y \partial_\nu \right] K_\mu + \text{H.c.}, \quad (5.12)$$

where  $Y$  stands for the isoscalar state  $\Lambda$  or isotriplet state  $\Sigma \cdot \boldsymbol{\tau}$ . Here, the  $\tau$  matrices operate to the isospin states of the nucleon and  $K$  or  $K^*$ . The follow-

ing axial-vector coupling constants involving  $K$  meson are derived from  $SU(3)$  symmetry relations:

$$g_{KN\Lambda} = -13.5, \quad g_{KN\Sigma} = 2.5, \quad (5.13)$$

where the coupling constants of baryon-baryon-meson vertices are represented in terms of the  $\pi NN$  coupling constant and the parameter  $\alpha$  (Rijken et al., 1999):

$$\frac{g_{KN\Lambda}}{g_{\pi NN}} = -\frac{1}{\sqrt{3}}(3 - 2\alpha), \quad (5.14)$$

$$\frac{g_{KN\Sigma}}{g_{\pi NN}} = -(1 - 2\alpha). \quad (5.15)$$

Here,  $g_{\pi NN} = 13$  denotes the coupling constant for the  $\pi NN$  vertex. The parameter  $\alpha = \frac{D}{F + D} \sim \frac{3}{5}$  is determined from the analysis of baryon-baryon interactions in a one-boson-exchange-potential approach (Nagels et al., 1979). The resulting numerical value is consistent with the results from the  $SU(6)$  symmetry (Pais, 1966) and large- $N_c$  analysis (Dashen et al., 1995). To express the finite size of hadrons, following form factors are included in our calculations:

$$F(t) = a^2 \frac{\Lambda^4}{\Lambda^4 + (t - m_\phi^2)^2}, \quad (5.16)$$

$$F_n(t) = a \left( \frac{\Lambda^2}{\Lambda^2 - t} \right)^n, \quad (n = 1, 2), \quad (5.17)$$

where  $t = q^2$  and  $m_\phi$  is the mass of the exchanged meson. Here, the form factor in Eq. (5.16) is multiplied to the whole Feynman amplitude (Kim et al., 2015; Nam et al., 2005; Haberzettl et al., 1998), while the second one in Eq. (5.17) is at each vertex. Therefore, in the Feynman amplitude, the normalization constant appears in  $a^2$  for both cases. Because there is always ambiguities in the use of form factors for such reaction processes, we will compare the results by using the

three different form factors.

The free model parameters are the vector coupling constant  $g_{K^*NY}$ , tensor coupling constant  $\kappa_{K^*NY}$ , normalization constant  $a$ , and cutoff parameter  $\Lambda$ . These parameters will be fixed by the existing observed data of relevant strangeness production cross sections. By applying Feynman rules to the effective Lagrangians in Eqs. (5.11) and (5.12), Feynman amplitudes of strangeness productions with  $K$  and  $K^*$  exchanges in the  $t$ -channel are given by

$$\mathcal{M}_K = \frac{g_{K^*NY} g_{KNY'}}{(m_N + m_Y)(m_N + m_{Y'})} \Gamma_N P_K(t) \Gamma_{\bar{N}}, \quad (5.18)$$

$$\mathcal{M}_{K^*} = g_{K^*NY} g_{K^*NY'} \Gamma_{N,\mu} P_{K^*}^{\mu\nu}(t) \Gamma_{\bar{N},\nu}, \quad (5.19)$$

where

$$\Gamma_N = i\bar{u}_Y \not{q} \gamma_5 u_N, \quad (5.20)$$

$$\Gamma_{\bar{N}} = -i\bar{v}_{\bar{N}} \not{q} \gamma_5 v_{\bar{Y}'}, \quad (5.21)$$

$$\Gamma_{N,\mu} = \bar{u}_Y \left[ (1 + \kappa_{K^*NY}) \gamma_\mu - \kappa_{K^*NY} \frac{(p_1 + p_3)_\mu}{m_N + m_Y} \right] u_N, \quad (5.22)$$

$$\Gamma_{\bar{N},\nu} = \bar{v}_{\bar{N}} \left[ (1 + \kappa_{K^*NY'}) \gamma_\nu + \kappa_{K^*NY'} \frac{(p_2 + p_4)_\nu}{m_N + m_{Y'}} \right] v_{\bar{Y}'}. \quad (5.23)$$

The Feynman propagators for  $K$  and  $K^*$  mesons are defined by

$$P_K(t) = \frac{i}{t - m_K^2}, \quad (5.24)$$

$$P_{K^*}^{\mu\nu}(t) = \frac{i(-g^{\mu\nu} + q^\mu q^\nu / m_{K^*}^2)}{t - m_{K^*}^2}. \quad (5.25)$$

The total Feynman amplitude is therefore written as

$$\mathcal{M}_{p\bar{p} \rightarrow Y\bar{Y}'} = \begin{cases} \mathcal{M}_K F_K + \mathcal{M}_{K^*} F_{K^*}, \\ \mathcal{M}_K F_{n,K}^2 + \mathcal{M}_{K^*} F_{n,K^*}^2. \end{cases} \quad (5.26)$$

Here  $F_{(K,K^*)}$  and  $F_{n,(K,K^*)}$  are form factors in Eqs. (5.16) and (5.17) with  $K$  or  $K^*$ , respectively. Differential cross section as a function of a momentum transfer  $t$  is computed from

$$\frac{d\sigma}{dt} = \frac{1}{64\pi (p_{cm})^2 s} \langle |\mathcal{M}|^2 \rangle, \quad (5.27)$$

where  $\langle |\mathcal{M}|^2 \rangle = \frac{1}{4} \sum_{s_3, s_4} |\mathcal{M}|^2$  and  $p_{cm}$  is the relative momentum of the proton and antiproton in the initial state in the center of mass frame. The spin projections of the outgoing hyperon and antihyperon are respectively denoted by  $s_3$  and  $s_4$ .

Now, we proceed to charm productions in  $p\bar{p}$  collisions. In principle, the coupling constants for charm and strange hadrons should be different. However, if strange and charm quarks are sufficiently heavy, the same set of coupling constants can be applied to charm productions. Therefore, the relevant Feynman amplitudes for the diagram in Figure 5.2 are obtained by replacing strange hadrons  $Y$ ,  $\bar{Y}'$ ,  $\phi$  by charmed hadrons  $Y_c$ ,  $\bar{Y}'_c$ ,  $\phi_c$ , ( $Y_c = \Lambda_c^+$ ,  $\Sigma_c^+$ ,  $\phi_c = \bar{D}^0$ ,  $\bar{D}^{*0}$ ).

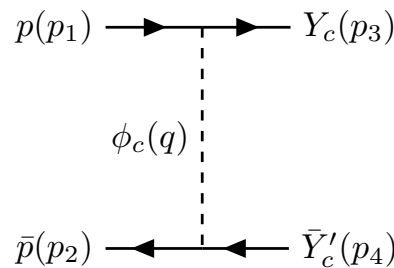


**Figure 5.2** Tree-level diagram for the reaction  $p\bar{p} \rightarrow Y_c\bar{Y}'_c$



### 5.3.2 Results for strangeness productions

In the following subsection, differential cross sections for strange baryons as functions of  $t_{max} - t$  are presented. In the observed differential cross sections of the reactions  $p\bar{p} \rightarrow \Lambda\bar{\Lambda}$  and  $p\bar{p} \rightarrow \Sigma\bar{\Lambda}$  (Becker et al., 1978), which exist only for  $p_{lab} = 6$  GeV, are composed of two distinct components: the steep component near the forward angle region and the less steep component in a finite angle region. In our case, the first component of the data is mainly focused due to the  $t$ -channel dominance. For a given energy, the value of  $t$  varies from  $t_{min}$  and  $t_{max}$  (i.e.,  $t_{max} - t$  varies from 0 to  $t_{max} - t_{min}$ ),

$$t_{max}^{min} = m_N^2 + m_Y^2 - \frac{1}{2s} \left[ s \left( s + m_Y^2 - m_{Y'}^2 \right) \pm \sqrt{s \left( s - 4m_N^2 \right) \left( s - \left( m_Y + m_{Y'} \right)^2 \right)} \right. \\ \left. \times \sqrt{\left( s - \left( m_Y - m_{Y'} \right)^2 \right)} \right]. \quad (5.28)$$

First, we try to fix the model parameters by comparing differential cross sections with the observed data for the reactions  $p\bar{p} \rightarrow \Lambda\bar{\Lambda}$  and  $p\bar{p} \rightarrow \Sigma\bar{\Lambda}$ . Then, differential cross sections for the reaction  $p\bar{p} \rightarrow \Sigma\bar{\Sigma}$  will be predicted. In each case, differential cross sections contributed by  $K$ ,  $K^*$ , and (total =  $K + K^*$ ) exchanges are displayed separately. Three distinct sets of results will be independently presented to demonstrate the influence of form factor dependency.

We start our discussion with the reaction  $p\bar{p} \rightarrow \Lambda\bar{\Lambda}$ . Since the coupling constants with  $K$  exchange in Eq. (5.13) have already been fixed by the  $SU(3)$  symmetry relations, the consistency between our results and the experimental data is established by appropriately determining the strengths of the unknown model parameters. To attain a satisfactory agreement with the data, we determine the

following parameters,

$$\begin{aligned}
 g_{K^*N\Lambda} &= -5.112, \quad \kappa_{K^*N\Lambda} = 2.037, \\
 F(t) : \quad a &= 0.46, \quad \Lambda = 0.63 \text{ GeV}, \\
 F_1(t) : \quad a &= 0.285, \quad \Lambda = 0.7 \text{ GeV}, \\
 F_2(t) : \quad a &= 0.285, \quad \Lambda = 0.99 \text{ GeV}.
 \end{aligned} \tag{5.29}$$

By using these parameters, differential cross sections for the reaction  $p\bar{p} \rightarrow \Lambda\bar{\Lambda}$  are displayed in Figure 5.3. In Figures 5.3a to 5.3c, we can observe the influence of the form factor dependency from the increasing steepness. The results shown in Figure 5.3b are in overall agreement with the data, whereas those in Figures 5.3a and 5.3c exhibit clear deviations from the data in the finite angle region. However, these results are consistent with the data near the forward angle region, where the dominance of  $t$ -channel dynamics is realized. Additionally, the strengths of the differential cross sections contributed by  $K$  exchange are approximately  $10^{-2}$  to  $10^{-3}$  times those of  $K^*$  exchange. Indeed, the dominance of  $K^*$  exchange over  $K$  exchange can be observed, and this tendency remains independent of the form factor.

Now, let us consider the reaction  $p\bar{p} \rightarrow \Sigma\bar{\Lambda}$ . To fit the existing experimental data, we have determined the following parameters:

$$g_{K^*N\Sigma} = -4.182, \quad \kappa_{K^*N\Sigma} = -0.688. \tag{5.30}$$

The resulting differential cross sections are presented in Figure 5.4, where we depict the outcomes obtained using different form factors: Figure 5.4a illustrates the results with the form factor  $F$  defined in Equation (5.16), which demonstrate

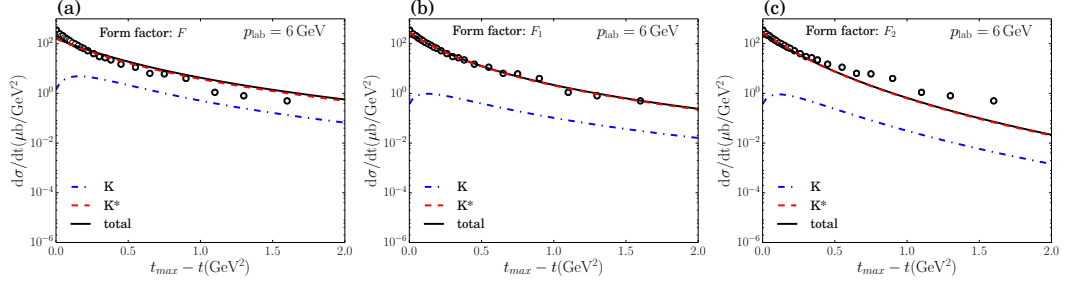


**Figure 5.3** Differential cross sections for the reaction  $p\bar{p} \rightarrow \Lambda\bar{\Lambda}$  at  $p_{lab} = 6$  GeV in the effective Lagrangian model. The circles denote the experimental data from Ref. (Becker et al., 1978).

an overall consistency with the data. However, noticeable deviations from the data are observed when the form factors  $F_1$  and  $F_2$  are utilized, as depicted in Figures 5.4b and 5.4c. Furthermore, it is worth noting that the cross sections involving  $K$  exchange are suppressed compared to those involving  $K^*$  exchange, by a factor similar to that observed in  $\Lambda\bar{\Lambda}$  production.

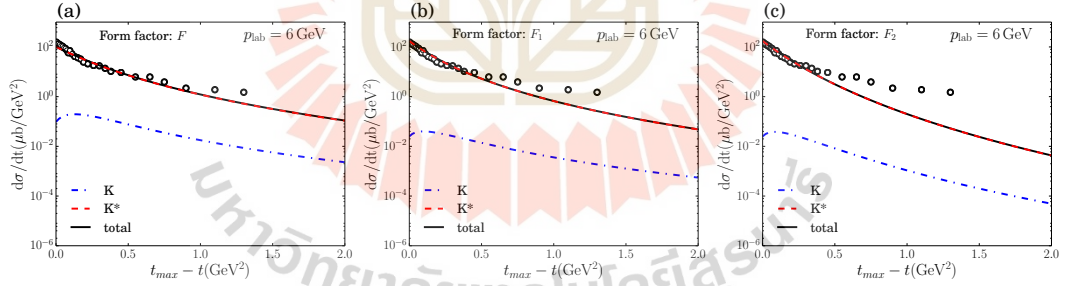


**Figure 5.4** Differential cross sections for the reaction  $p\bar{p} \rightarrow \Sigma\bar{\Lambda}$  at  $p_{lab} = 6$  GeV in the effective Lagrangian model. The circles denote the experimental data from Ref. (Becker et al., 1978).

By employing the model parameters determined from the two previous reactions, we can predict the differential cross sections for the reaction  $p\bar{p} \rightarrow \Sigma\bar{\Sigma}$ , as shown in Figure 5.5. In this case, the results contributed by  $K$  exchange are significantly smaller, approximately  $10^{-5}$  times, compared to those of  $K^*$  exchange.

This suppression is larger than those of  $\Lambda\bar{\Lambda}$  and  $\Sigma\bar{\Lambda}$  productions. When comparing the three cases of  $\Lambda\bar{\Lambda}$ ,  $\Sigma\bar{\Lambda}$ , and  $\Sigma\bar{\Sigma}$  productions, we observe that the magnitudes of the strange production cross sections decrease as the total mass in the final state becomes larger.

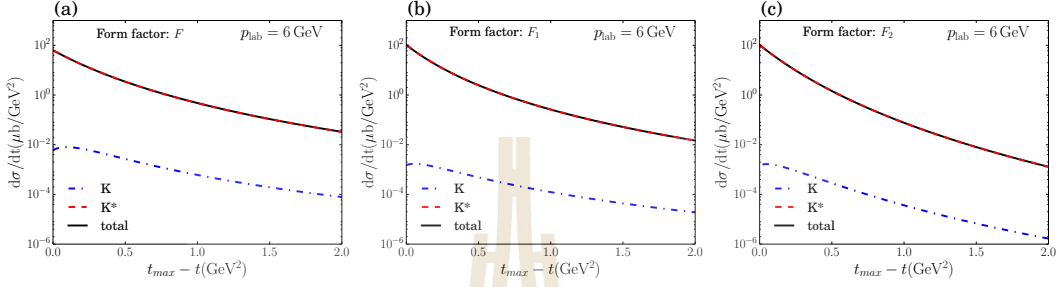


**Figure 5.5** Differential cross sections for the reaction  $p\bar{p} \rightarrow \Sigma\bar{\Sigma}$  at  $p_{lab} = 6$  GeV in the effective Lagrangian model.

### 5.3.3 Predictions for charm productions

In this subsection, we discuss differential cross sections for various charm productions. The results for the reactions  $p\bar{p} \rightarrow \Lambda_c\bar{\Lambda}_c$ ,  $p\bar{p} \rightarrow \Sigma_c\bar{\Lambda}_c$ , and  $p\bar{p} \rightarrow \Sigma_c\bar{\Sigma}_c$  at  $p_{lab} = 15$  GeV are presented in Figures 5.6 to 5.8.

According to our predictions, the charm production differential cross sections are mainly contributed by vector  $D^*$  exchange, as their magnitudes are almost similar to those of  $D + D^*$  exchange. Different types of form factors result in different slopes and absolute values of charm production cross sections, as depicted in Figures 5.6 to 5.8. The slopes of charm production rates exhibit similar tendencies as those of strangeness productions, since only the kinematic parameters for strange hadrons have been replaced by those of charm, while other parameters such as coupling constants and those of form factors remain unchanged.

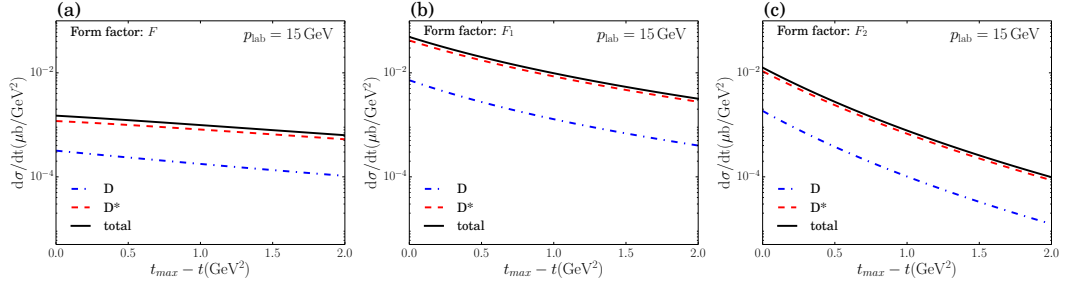


**Figure 5.6** Differential cross sections for the reaction  $p\bar{p} \rightarrow \Lambda_c \bar{\Lambda}_c$  at  $p_{\text{lab}} = 15 \text{ GeV}$  in the effective Lagrangian model.

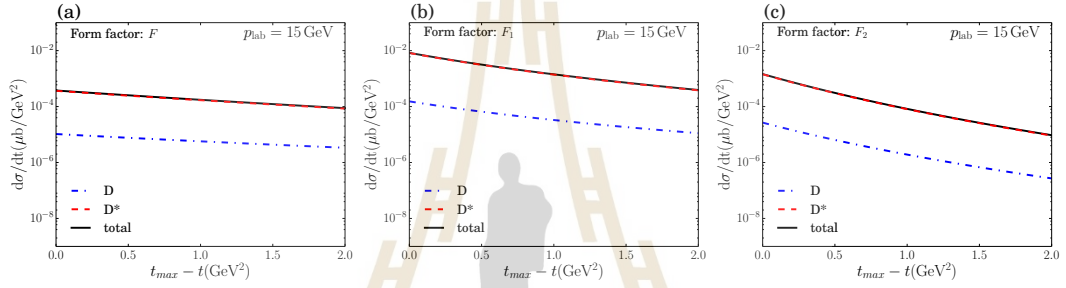


**Figure 5.7** Differential cross sections for the reaction  $p\bar{p} \rightarrow \Sigma_c \bar{\Lambda}_c$  at  $p_{\text{lab}} = 15 \text{ GeV}$  in the effective Lagrangian model.

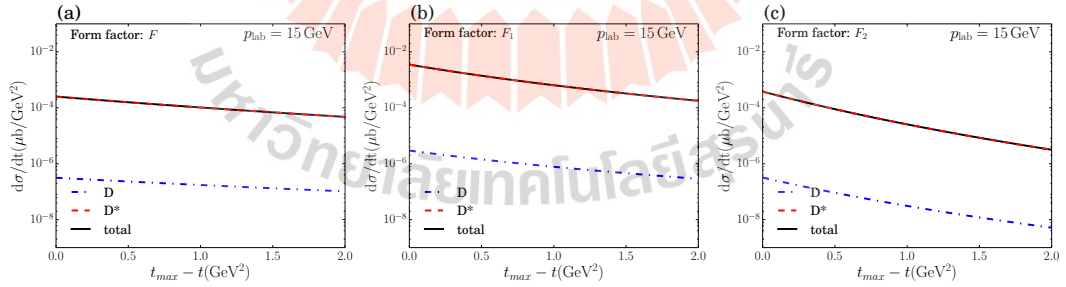


**Figure 5.8** Differential cross sections for the reaction  $p\bar{p} \rightarrow \Sigma_c \bar{\Sigma}_c$  at  $p_{\text{lab}} = 15 \text{ GeV}$  in the effective Lagrangian model.

In the reaction  $p\bar{p} \rightarrow \Lambda_c \bar{\Lambda}_c$ , the absolute values of the production rates depicted in Figures 5.6b and 5.6c are roughly at the same order, whereas those in Figure 5.6a are significantly suppressed. This indicates that the largest suppression

is observed when using the form factor  $F$ , while the form factors  $F_1$  and  $F_2$  result in lower suppressions of the production rates. This behavior can also be observed in the reactions  $p\bar{p} \rightarrow \Sigma_c \bar{\Lambda}_c$  and  $p\bar{p} \rightarrow \Sigma_c \bar{\Sigma}_c$ . The cross section values range from  $10^{-2}$  to  $10^{-4} \mu\text{b}/\text{GeV}^2$ , and they are approximately  $10^{-2}$  to  $10^{-4}$  times those of the reaction  $p\bar{p} \rightarrow \Lambda \bar{\Lambda}$ .

In the reaction  $p\bar{p} \rightarrow \Sigma_c \bar{\Lambda}_c$ , the form factor dependence displayed in Figure 5.7 is similar to that observed in the  $p\bar{p} \rightarrow \Sigma \bar{\Lambda}$  reaction, as compared to Figure 5.4. The predicted cross section values range from approximately  $10^{-3}$  to  $10^{-5} \mu\text{b}/\text{GeV}^2$ , and they are about  $10^{-2}$  to  $10^{-5}$  times those of the reaction  $p\bar{p} \rightarrow \Sigma \bar{\Lambda}$ . Regarding the reaction  $p\bar{p} \rightarrow \Sigma_c \bar{\Sigma}_c$ , as shown in Figure 5.8, the predicted cross section values are approximately  $10^{-3}$  to  $10^{-6} \mu\text{b}/\text{GeV}^2$ , and they are suppressed compared to the cross sections of the  $p\bar{p} \rightarrow \Sigma \bar{\Sigma}$  reaction by a factor similar to that observed in the  $p\bar{p} \rightarrow \Sigma_c \bar{\Lambda}_c$  reaction.

Indeed, the predicted charm production cross sections obtained from the effective Lagrangian approach exhibit magnitudes ranging from  $10^{-2}$  to  $10^{-6} \mu\text{b}/\text{GeV}^2$ , with corresponding suppression factors ranging from  $10^{-2}$  to  $10^{-5}$ . These magnitudes are consistent with the results obtained in previous studies, such as those presented in Refs. (Titov and Kampfer, 2008; Khodjamirian et al., 2012), which were performed within the Regge approach. The Regge theory is well known for its ability to reproduce the energy dependence of differential cross sections at high energies. Therefore, in order to ensure that the magnitudes of the production rates obtained from the effective Lagrangian calculations are of the same order as those implied by Regge theory, the form factor  $F$  is included in the entire amplitude, rather than at each vertex. A similar treatment for the form factor  $F$  was employed in Ref. (Kim et al., 2015) to investigate charm productions from pion-induced reactions within the effective Lagrangian approach.

## 5.4 Regge approach

### 5.4.1 Amplitudes

The Regge amplitudes are obtained by replacing the propagator in the Feynman amplitudes by the Regge propagator,

$$\mathcal{M}_{K_R} = \mathcal{M}_K (t - m_K^2) P_K^R(s, t), \quad (5.31)$$

$$\mathcal{M}_{K_R^*} = \mathcal{M}_{K^*} (t - m_{K^*}^2) P_{K^*}^R(s, t), \quad (5.32)$$

where  $P_K^R(s, t)$  and  $P_{K^*}^R(s, t)$  are the Regge propagators for  $K$  and  $K^*$  Reggeons, respectively. These Regge propagators are written by (Kim et al., 2015)

$$P_K^R(s, t) = \Gamma[-\alpha_K(t)] \alpha'_K \left( \frac{s}{S_K} \right)^{\alpha_K(t)}, \quad (5.33)$$

$$P_{K^*}^R(s, t) = \Gamma[1 - \alpha_{K^*}(t)] \alpha'_{K^*} \left( \frac{s}{S_{K^*}} \right)^{\alpha_{K^*}(t)-1}. \quad (5.34)$$

Here the Regge trajectories for  $\alpha_K$  and  $\alpha_{K^*}$  are given by (Brisudova et al., 2000)

$$\alpha_K(t) = -0.15 + 0.62t, \quad (5.35)$$

$$\alpha_{K^*}(t) = 0.41 + 0.71t. \quad (5.36)$$

In Eqs. (5.33) and (5.34), the scaling parameters for  $K$  and  $K^*$  Reggeon exchanges are  $S_K = 2.42 \text{ GeV}^2$  and  $S_{K^*} = 2.45 \text{ GeV}^2$ . At high energies, the imaginary part of the inelastic scattering amplitude can be factorized into a product of two elastic scattering amplitudes. This factorization property allows for the evaluation of scaling and Regge parameters for different inelastic scatterings. Near the Regge pole of the ground state on a specific trajectory, the behavior of the Feynman propagator can be approximated by the corresponding  $\Gamma$ -function in the Regge

propagator, i.e.,

$$\Gamma(1 - \alpha_{K^*}(t)) \simeq -\frac{1}{\alpha'_{K^*}(t - m_{K^*}^2)}. \quad (5.37)$$

In addition to the above prescription, the following overall residual factor which accounts for the non-point-like nature of hadrons and incorporates the effects of their internal structure,

$$C(t) = \frac{b}{\left(1 - \frac{t}{\Lambda^2}\right)^2}, \quad (5.38)$$

is introduced to improve  $t$ -dependences of the Regge amplitudes. There are two unknown parameters in this residual factor: overall constant  $b$  and cutoff parameter  $\Lambda$ . These parameters will be fixed by comparing differential cross sections with the experimental data for strangeness productions. The total Regge amplitude of the reaction  $p\bar{p} \rightarrow Y\bar{Y}'$  is written by

$$\mathcal{M}_{p\bar{p} \rightarrow Y\bar{Y}'}^R = C(t) \left( \mathcal{M}_K^R + \mathcal{M}_{K^*}^R \right). \quad (5.39)$$

To predict production rates of the reaction  $p\bar{p} \rightarrow Y_c\bar{Y}'_c$ , the following Regge propagators and scaling parameters for  $D$  and  $D^*$  Reggeons are used (Brisudova et al., 2000)

$$P_D^R(s, t) = \Gamma[-\alpha_D(t)] \alpha'_D \left(\frac{s}{s_D}\right)^{\alpha_D(t)}, \quad (5.40)$$

$$P_{D^*}^R(s, t) = \Gamma[1 - \alpha_{D^*}(t)] \alpha'_{D^*} \left(\frac{s}{s_{D^*}}\right)^{\alpha_{D^*}(t)-1}, \quad (5.41)$$

where

$$\alpha_D(t) = -1.61 + 0.44t, \quad (5.42)$$

$$\alpha_{D^*}(t) = -1.02 + 0.47t. \quad (5.43)$$



In Eqs. (5.40) and (5.41), the scaling parameters for  $D$  and  $D^*$  Reggeon exchanges are  $S_D = 5.46 \text{ GeV}^2$  and  $S_{D^*} = 6.01 \text{ GeV}^2$ . The Regge formalism is consistent with the conservation of unitarity, allowing for the reproduction of the tendencies observed in scattering cross sections, particularly in the forward angle region. As  $s \rightarrow \infty$ , the asymptotic behavior of the differential cross sections, as given in Eq. (5.10), is guaranteed.

However, in our construction of the Regge amplitudes using the vertex structure of the Feynman amplitudes, the asymptotic behavior at  $s \rightarrow \infty$  may not be automatically satisfied. To address this issue, we introduce a normalization factor in accordance with the approach presented in Ref. (Titov and Kampf, 2008).

$$\mathcal{N}(s, t) = \frac{A^\infty(s)}{A(s, t)}, \quad A^2(s, t) = \sum_{s_3, s_4} |M(s, t)|^2. \quad (5.44)$$

The function  $M(s, t)$  is obtained by removing the denominator of the Feynman propagator in the Feynman amplitude  $\mathcal{M}$ . The term  $A^\infty(s)$  represents the leading contribution in  $M(s, t)$  as  $s \rightarrow \infty$ . It captures the dominant behavior of the amplitude at high energies, providing important information about the scattering process in the asymptotic limit. For pseudoscalar Reggeon exchange, we get  $A^\infty(s) = 2(m_N - m_Y)(m_{\bar{N}} - m_{\bar{Y}'})$  while  $A^\infty(s) = 4s$  is obtained for vector Reggeon exchange. Therefore, Regge amplitude in Eq. (5.39) is then rewritten by

$$\mathcal{M}_{p\bar{p} \rightarrow Y\bar{Y}'}^R = C(t) \left( \mathcal{N}_K(s, t) \mathcal{M}_K^R + \mathcal{N}_{K^*}(s, t) \mathcal{M}_{K^*}^R \right). \quad (5.45)$$

This form of the Regge amplitude is then consistent with the asymptotic condition in Eq. (5.10).

Finally, we determine the overall constant  $b$  and the cutoff  $\Lambda$  in the form factor  $C(t)$  to reproduce the magnitudes of the  $p\bar{p} \rightarrow \Lambda\bar{\Lambda}$  and  $p\bar{p} \rightarrow \Sigma\bar{\Lambda}$  cross

sections. The obtained values are:

$$C(t) : b = 0.25, \Lambda = 1.1 \text{ GeV}. \quad (5.46)$$

These values of  $b$  and  $\Lambda$  are chosen to ensure a good agreement between the calculated cross sections and the experimental data for the corresponding reactions.

## 5.4.2 Results for strangeness productions

The differential cross sections are presented in Figure 5.9. When compared to the experimental data in Figures 5.9a and 5.9b, we observe an overall agreement at a similar level to the effective Lagrangian approach. Particularly, the slopes of the two data sets are well reproduced near the forward angle region. However, for large values of  $t$ , the calculations underestimate the data. Consistent with our previous findings, the vector  $K^*$  Reggeon contribution dominates over the  $K$  Reggeon contribution. In the Regge model, it is evident that the  $K$  Reggeon is more suppressed as the final state becomes heavier ( $K(\Lambda\bar{\Lambda}) > K(\Sigma\bar{\Lambda}) > K(\Sigma\bar{\Sigma})$ ).

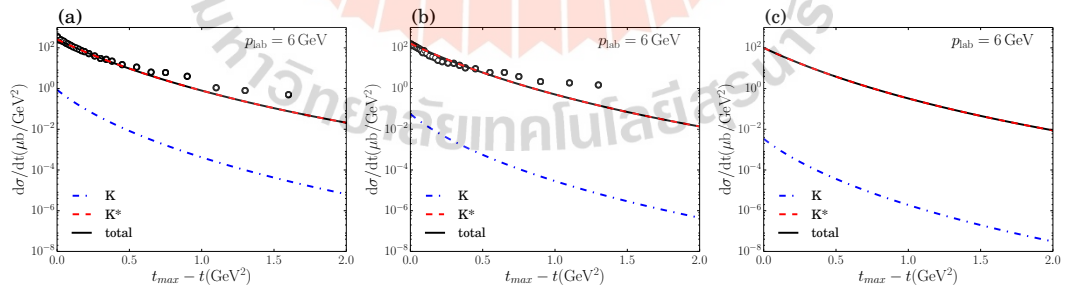


**Figure 5.9** Differential cross sections for the reactions (a)  $p\bar{p} \rightarrow \Lambda\bar{\Lambda}$ , (b)  $p\bar{p} \rightarrow \Sigma\bar{\Lambda}$ , and (c)  $p\bar{p} \rightarrow \Sigma\bar{\Sigma}$  at  $p_{lab} = 6 \text{ GeV}$  in the Regge model. The circles denote the experimental data from Ref.(Becker et al., 1978).

### 5.4.3 Predictions for charm productions

By applying the same set of parameters for the form factor  $C(t)$  and coupling constants, we can predict charm production cross sections in the Regge approach. The results are presented in Figure 5.10 for  $p_{\text{lab}} = 15$  GeV. As observed, the charm production cross sections are suppressed compared to strangeness productions by a similar amount as seen in the effective Lagrangian approach (refer to Figures 5.6 to 5.8). Similar to strangeness production, the dominant contribution comes from the  $D^*$  (vector) Reggeon, while the  $D$  (pseudoscalar) Reggeon contribution is highly suppressed. The magnitudes of the differential cross sections range from  $10^{-2}$  to  $10^{-4} \mu\text{b}/\text{GeV}^2$  near the forward angle region, which aligns with the results obtained in Refs. (Titov and Kampfer, 2008; Khodjamirian et al., 2012).

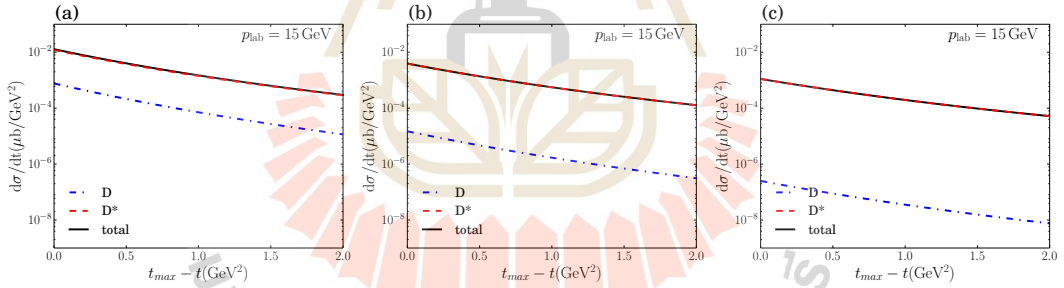


**Figure 5.10** Differential cross sections for the reactions (a)  $p\bar{p} \rightarrow \Lambda_c \bar{\Lambda}_c$ , (b)  $p\bar{p} \rightarrow \Sigma_c \bar{\Lambda}_c$ , and (c)  $p\bar{p} \rightarrow \Sigma_c \bar{\Sigma}_c$  at  $p_{\text{lab}} = 15$  GeV in the Regge model.

## 5.5 Total cross sections

In Figure 5.11, the total cross sections for different strangeness and charm productions are presented as functions of  $s/s_{\text{th}}$ , where  $s_{\text{th}} = (m_Y + m_{\bar{Y}})^2$ . These results are obtained using the effective Lagrangian model with the form factor  $F$

given by Eq. (5.16). The figure shows the following production rates: (a)  $\Lambda\bar{\Lambda}$  and  $\Lambda_c\bar{\Lambda}_c$ , (b)  $\Sigma\bar{\Lambda}$  and  $\Sigma_c\bar{\Lambda}_c$ , and (c)  $\Sigma\bar{\Sigma}$  and  $\Sigma_c\bar{\Sigma}_c$ .

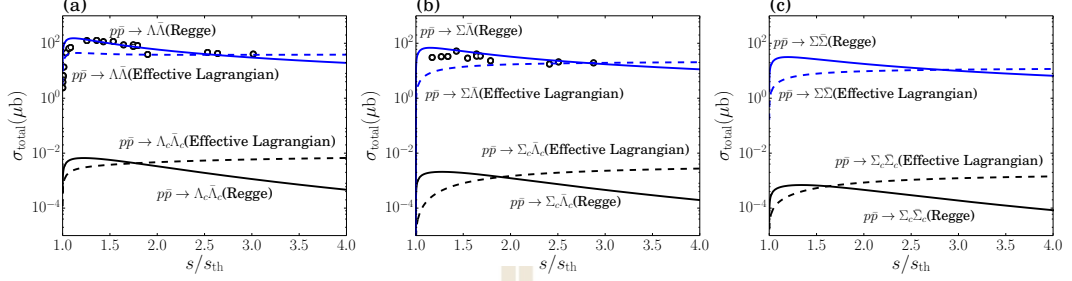


**Figure 5.11** Total cross sections for the reactions (a)  $p\bar{p} \rightarrow \Lambda\bar{\Lambda}$  and  $p\bar{p} \rightarrow \Lambda_c\bar{\Lambda}_c$ , (b)  $p\bar{p} \rightarrow \Sigma\bar{\Lambda}$  and  $p\bar{p} \rightarrow \Sigma_c\bar{\Lambda}_c$ , and (c)  $p\bar{p} \rightarrow \Sigma\bar{\Sigma}$  and  $p\bar{p} \rightarrow \Sigma_c\bar{\Sigma}_c$ . The circles are the experimental data from Refs. (Becker et al., 1978; Barnes et al., 1989; Barnes et al., 1991; Barnes et al., 1996).

The figures show that the total cross sections predicted by the two approaches exhibit similar overall behavior. There is a point of intersection at an intermediate energy for all cases, such as  $s/s_{th} \sim 2.7$  GeV for  $\Lambda\bar{\Lambda}$  production. This crossing point is a result of parameter choices that were made to reproduce the experimental data at that specific energy. Below the crossing point, the Regge model predicts larger cross section values compared to the effective Lagrangian model, while above the crossing point, the order is reversed. At high energies, the Regge model successfully captures the expected decrease in the cross section. Overall, the Regge model provides a better reproduction of the energy dependence compared to the effective Lagrangian model. However, it should be noted that the Regge model tends to overestimate the cross sections near the threshold region. This discrepancy can be attributed to the presence of strong final state interactions at low energies (Larionov and Lenske, 2017), particularly near the threshold, which have not been considered in the present work. In reality, baryon-antibaryon

annihilation can occur, leading to a partial loss of the initial flux.

Despite the difference in energy dependences in the two approaches, we have found that the production rates of charmed baryons are about  $10^{-4}$  -  $10^{-6}$  times those of hyperon productions, depending on the produced baryons and energies. As a typical energy around  $s/s_{th} \sim 1.5 - 2.0$ , the reduction rate is about  $10^{-5}$ .

In Ref. (Haidenbauer et al., 1992), different cutoff parameter for  $KN\Lambda$  and  $K^*N\Lambda$  vertices is employed for the total cross sections of  $p\bar{p} \rightarrow \Lambda\bar{\Lambda}$  near the threshold,  $\Lambda_{KN\Lambda} = \Lambda_{K^*N\Lambda} = 1.2$  GeV. In our present approach, if we employ these larger cutoff parameters, we need to reduce the strengths of the coupling constants, in particular the dominant one for the  $K^*$  meson, to reproduce the observed total cross sections. However, the  $t$ -dependence of  $d\sigma/dt$  at  $p_L = 6$  GeV cannot be reproduced well in this case. Furthermore, when extending their calculations to the charm sector (Haidenbauer and Krein, 2017), a larger cutoff parameter of 3 GeV was employed. As a result, they have significantly larger production rates for the charmed baryon productions, typically  $10^{-1}$  times strangeness production rates. If we consider the physical meaning of the cutoff as related to the hadron size  $\sim 1$  fm, it is reasonable to employ a cutoff of order 1 GeV that leads to the suppression of order  $10^{-4} - 10^{-5}$ .

# CHAPTER VI

## SUMMARY

We have constructed the effective Lagrangians for  $D$ -mesons, charmed, and light baryons, which are invariant under isospin, chiral, discrete, and Lorentz symmetries. The resulting Lagrangian comprises fifteen terms at the chiral orders  $\mathcal{O}(q^0)$  and  $\mathcal{O}(q)$ . To enhance the model's predictive power, we employ heavy quark symmetry and large- $N_c$  analysis to reduce the number of model parameters. Seven free parameters remain after the heavy quark symmetry constraints, while six free parameters are implied by large- $N_c$  constraints. The combined constraints from heavy quark and large- $N_c$  analyses imply five free parameters. We estimate the coupling constants for the effective Lagrangians by investigating the various decay modes of  $\Lambda_c$  and  $\Sigma_c$  baryons using the effective Lagrangian method and quark model.

We then investigate strangeness and charm productions using effective Lagrangian and Regge models. We formulate an effective Lagrangian model where parameters and form factors are determined using various symmetry relations and experimental data for strangeness productions, including  $d\sigma/dt$  at  $p_{\text{lab}} = 6$  GeV and the total cross sections  $\sigma$  at various energies. Our model explains both  $d\sigma/dt$  and  $\sigma$  reasonably well. We then apply the model to the charm sector, where we predict that the production rates are about  $10^{-4}$  to  $10^{-5}$  times those of strangeness productions.

We perform a similar analysis in the Regge model, where we use the same strategy as for the strangeness sector. We find that the resulting  $d\sigma/dt$  and  $\sigma$

agree reasonably well with data, and the Regge model provides a better fit for the experimental data in the large energy region. We also find that the charm production rates are similar to those obtained using the effective Lagrangian approach for  $s/s_{th} \lesssim 2$ . For the higher energy region, the Regge model predicts a better decreasing tendency as it obeys the unitarity bound. Similar tendencies were reported in previous investigations of pion-induced productions of charmed baryons (Kim et al., 2015).

After conducting a systematic and inclusive study in these two approaches, we find that the charm production rate in  $p\bar{p}$  collision is approximately  $10^{-4}$  to  $10^{-5}$  times that of strangeness in the energy region  $s/s_{th} \sim 1.5 - 2$ . Therefore, the expected total cross sections vary from  $10^{-2}\mu b$  to  $10^{-4}\mu b$ , which is our probable prediction.

The presently developed High-Energy Storage Ring (HESR) of FAIR is to store antiproton in the momentum range from 1.5 to 15 GeV/c, and in the future the Ring may be developed to a collider mode at  $\sqrt{s}$  up to 32 GeV. A conservative estimation of the  $\bar{p}$  luminosity which can be reached at the startup phase is  $4 \times 10^{30} \text{ cm}^{-2}\text{s}^{-1}$ . One may use this luminosity to estimate the significant event rates for our predicted cross sections for 1 year ( $10^7 \text{ s}$ ) running of PANDA experiment (Frankfurt et al., 2020). For the maximum beam momentum (15 GeV/c;  $\sqrt{s} = 5.474 \text{ GeV}$ ), the  $s/s_{th}$  are about 1.43, 1.33, and 1.24 for  $\Lambda_c\bar{\Lambda}_c$ ,  $\Lambda_c\bar{\Sigma}_c$ , and  $\Sigma_c\bar{\Sigma}_c$  channels, respectively. At  $s/s_{th} = 1.2 - 1.5$ , the total cross sections vary from  $10^{-2} \mu b$  to  $10^{-4} \mu b$  for the  $p\bar{p} \rightarrow \Lambda_c\bar{\Lambda}_c$ ,  $\Lambda_c\bar{\Sigma}_c$  and  $\Sigma_c\bar{\Sigma}_c$  reactions, which correspond to the significant event rates from  $10^6$  and  $10^4$  for 1 year ( $10^7 \text{ s}$ ) at the luminosity  $4 \times 10^{30} \text{ cm}^{-2}\text{s}^{-1}$ . With such event rates, one may comfortably measure the cross sections. In addition, one is able to intensively perform the analysis for angular distributions of charm production rates since the typical range of  $t$  is about

-1.14 to -16.62 GeV<sup>2</sup>. If this is the case, we expect even more abundant productions for excited charmed baryons as suggested in Ref. (Shim et al., 2020). Therefore,  $p\bar{p}$  process will be useful to explore further the nature of charmed baryons.







**REFERENCES**

## REFERENCES

- Aaij, R., Abellan Beteta, C., Adeva, B., Adinolfi, M., Adrover, C., Affolder, A., Ajaltouni, Z., Albrecht, J., Alessio, F., Alexander, M., Ali, S., Alkhazov, G., Alvarez Cartelle, P., Alves, A. A., Amato, S., et al. (2013). Determination of the X(3872) meson quantum numbers. **Phys. Rev. Lett.**, 110:222001.
- Aaij, R., Adeva, B., Adinolfi, M., Affolder, A., Ajaltouni, Z., Albrecht, J., Alessio, F., Alexander, M., Ali, S., Alkhazov, G., Alvarez Cartelle, P., Alves, A. A., Amato, S., Amerio, S., Amhis, Y., et al. (2014). Observation of the resonant character of the  $Z(4430)^-$  state. **Phys. Rev. Lett.**, 112(22):222002.
- Abe, K., Adachi, I., Aihara, H., Arinstein, K., Asano, Y., Aulchenko, V., Aushev, T., Aziz, T., Bakich, A. M., Balagura, V., Barbero, M., Bedny, I., Bitenc, U., Bizjak, I., Bondar, A., et al. (2007). Observation of a new charmonium state in double charmonium production in  $e^+e^-$  annihilation at  $\sqrt{s} \approx 10.6$  GeV. **Phys. Rev. Lett.**, 98:082001.
- Ablikim, M., Achasov, M. N., Ai, X. C., Albayrak, O., Ambrose, D. J., An, F. F., An, Q., Bai, J. Z., Baldini Ferroli, R., Ban, Y., Becker, J., Bennett, J. V., Bertani, M., Bian, J. M., Boger, E., et al. (2013a). Observation of a charged charmoniumlike structure in  $e^+e^- \rightarrow \pi^+\pi^- J/\psi$  at  $\sqrt{s} = 4.26$  GeV. **Phys. Rev. Lett.**, 110:252001.
- Ablikim, M., Achasov, M. N., Albayrak, O., Ambrose, D. J., An, F. F., An, Q., Bai, J. Z., Baldini Ferroli, R., Ban, Y., Becker, J., Bennett, J. V., Bertani, M.,

- Bian, J. M., Boger, E., Bondarenko, O., et al. (2013b). Observation of a charged charmoniumlike structure  $Z_c(4020)$  and search for the  $Z_c(3900)$  in  $e^+e^- \rightarrow \pi^+\pi^-h_c$ . **Phys. Rev. Lett.**, 111(24):242001.
- AlFiky, M. T., Gabbiani, F., and Petrov, A. A. (2006).  $X(3872)$ : Hadronic molecules in effective field theory. **Phys. Lett. B**, 640:238–245.
- Aubert, B., Barate, R., Boutigny, D., Couderc, F., Gaillard, J.-M., Hicheur, A., Karyotakis, Y., Lees, J. P., Tisserand, V., Zghiche, A., Palano, A., Pompili, A., Chen, J. C., Qi, N. D., Rong, G., et al. (2005a). Study of the  $B \rightarrow J/\psi K^- \pi^+ \pi^-$  decay and measurement of the  $B \rightarrow X(3872) K^-$  branching fraction. **Phys. Rev. D**, 71:071103.
- Aubert, B., Barate, R., Boutigny, D., Couderc, F., Karyotakis, Y., Lees, J. P., Poireau, V., Tisserand, V., Zghiche, A., Grauges, E., Palano, A., Pappagallo, M., Pompili, A., Chen, J. C., Qi, N. D., et al. (2005b). Observation of a broad structure in the  $\pi^+\pi^- J/\psi$  mass spectrum around 4.26 GeV/c<sup>2</sup>. **Phys. Rev. Lett.**, 95:142001.
- Aubert, J. J., Becker, U., Biggs, P. J., Burger, J., Chen, M., Everhart, G., Goldhagen, P., Leong, J., McCorriston, T., Rhoades, T. G., Rohde, M., Ting, S. C. C., Wu, S. L., and Lee, Y. Y. (1974). Experimental Observation of a Heavy Particle J. **Phys. Rev. Lett.** 33: 1404–1406.
- Augustin, J. E., Boyarski, A. M., Breidenbach, M., Bulos, F., Dakin, J. T., Feldman, G. J., Fischer, G. E., Fryberger, D., Hanson, G., Jean-Marie, B., Larsen, R. R., Lueth, V., Lynch, H. L., Lyon, D., Morehouse, C. C., et al. (1974). Discovery of a narrow resonance in  $e^+e^-$  annihilation. **Phys. Rev. Lett.** 33: 1406–1408.

- Azizi, K., Sarac, Y., and Sundu, H. (2014). Strong  $\Lambda_b NB$  and  $\Lambda_c ND$  vertices. **Phys. Rev. D**, 90(11):114011.
- Azizi, K., Sarac, Y., and Sundu, H. (2015a). Strong couplings of negative and positive parity nucleons to the heavy baryons and mesons. **Phys. Rev. D**, 92(1):014022.
- Azizi, K., Sarac, Y., and Sundu, H. (2015b). Strong  $\Sigma_b NB$  and  $\Sigma_c ND$  coupling constants in QCD. **Nucl. Phys. A**, 943:159–167.
- Barnes, P. D., Besold, R., Birien, P., Bonner, B., Breunlich, W., Diebold, G., Dutty, W., Eisenstein, R., Ericsson, G., Eyrich, W., Von Frankenberg, R., Franklin, G., Franz, J., Hamann, N., Hertzog, D., et al. (1989). Threshold measurement of the reaction  $p\bar{p} \rightarrow \Lambda\bar{\Lambda}$  at LEAR. **Phys. Lett. B**, 229:432–438.
- Barnes, P. D., Diebold, G., Franklin, G., Maher, C., Quinn, B., Seydoux, J., Kilian, K., Besold, R., Eyrich, W., Von Frankenberg, R., Hofmann, A., Malz, D., Stinzing, F., Woldt, P., Birien, P., et al. (1991). Study of the reaction  $p\bar{p} \rightarrow \Lambda\bar{\Lambda}$  at 1.546 GeV/c and 1.695 GeV/c. **Nucl. Phys. A**, 526:575–601.
- Barnes, P. D., Diebold, G., Franklin, G., Quinn, B., Schumacher, R., Seydoux, J., Zeps, V., Birien, P., Dutty, W., Fischer, H., Franz, J., Rössle, E., Schlegelmann, H., Schmitt, H., Todenhagen, R., et al. (1996). Observables in high statistics measurements of the reaction  $p\bar{p} \rightarrow \Lambda\bar{\Lambda}$ . **Phys. Rev. C**, 54:1877–1886.
- Becker, H., Blunar, G., Blum, W., Chabaud, V., De Groot, J., Dietl, H., Gallivan, J., Kern, W., Lorenz, E., Lütjens, G., Lutz, G., Männer, W., Mount,

- R., Notz, D., Richter, R., et al. (1978). Measurement of the reactions  $\bar{p}p \rightarrow \bar{\Lambda}\Lambda$ ,  $\bar{p}p \rightarrow \bar{\Lambda}\Sigma^0$  and  $\bar{p}p \rightarrow \bar{\Lambda}$  (Missing mass) at 6 GeV. **Nucl. Phys. B**, 141:48–64.
- Braguta, V. V., Likhoded, A. K., and Luchinsky, A. V. (2005). Excited charmonium mesons production in  $e^+e^-$  annihilation at  $\sqrt{s} = 10.6$  GeV. **Phys. Rev. D**, 72:074019.
- Brambilla, N., Eidelman, S., Heltsley, B. K., Vogt, R., Bodwin, G. T., Eichten, E., Frawley, A. D., Meyer, A. B., Mitchell, R. E., Papadimitriou, V., Petreczky, P., Petrov, A. A., Robbe, P., Vairo, A., Andronic, A., et al. (2011). Heavy quarkonium: progress, puzzles, and opportunities. **Eur. Phys. J. C**, 71:1534.
- Brambilla, N., Pineda, A., Soto, J., and Vairo, A. (2000). Potential NRQCD: an effective theory for heavy quarkonium. **Nucl. Phys. B**, 566:275.
- Brisudova, M. M., Burakovsky, L., and Goldman, J. T. (2000). Effective functional form of Regge trajectories. **Phys. Rev. D**, 61:054013.
- Casalbuoni, R., Deandrea, A., Di Bartolomeo, N., Gatto, R., Feruglio, F., and Nardulli, G. (1997). Phenomenology of heavy meson chiral Lagrangians. **Phys. Rept.**, 281:145–238.
- Cazzoli, E. G., Cnops, A. M., Connolly, P. L., Louttit, R. I., Murtagh, M. J., Palmer, R. B., Samios, N. P., Tso, T. T., and Williams, H. H. (1975). Evidence for  $\Delta S = -\Delta Q$  currents or charmed baryon production by neutrinos. **Phys. Rev. Lett.**, 34:1125–1128.
- Chen, P. (2001). Heavy quarks on anisotropic lattices: the charmonium spectrum. **Phys. Rev. D**, 64:034509.

- Chiu, T. W. and Hsieh, T. H. (2006).  $Y(4260)$  on the lattice. **Phys. Rev. D**, 73:094510.
- Chiu, T. W. and Hsieh, T. H. (2007).  $X(3872)$  in lattice QCD with exact chiral symmetry. **Phys. Lett. B**, 646:95–99.
- Cho, P. L. (1992). Chiral perturbation theory for hadrons containing a heavy quark: The Sequel. **Phys. Lett. B**, 285:145–152.
- Choi, S. K., Olsen, S. L., Abe, K., Abe, T., Adachi, I., Ahn, B. S., Aihara, H., Akai, K., Akatsu, M., Akemoto, M., Asano, Y., Aso, T., Aulchenko, V., Aushev, T., Bakich, A. M., et al. (2003). Observation of a narrow charmonium-like state in exclusive  $B^\pm \rightarrow K^\pm \pi^+ \pi^- J/\psi$  decays. **Phys. Rev. Lett.**, 91:262001.
- Choi, S. K., Olsen, S. L., Adachi, I., Aihara, H., Aulchenko, V., Aushev, T., Aziz, T., Bakich, A. M., Balagura, V., Bedny, I., Bitenc, U., Bondar, A., Bozek, A., Bračko, M., Brodzicka, J., et al. (2008). Observation of a resonance-like structure in the  $\pi^\pm \psi'$  mass distribution in exclusive  $B \rightarrow K \pi^\pm \psi'$  decays. **Phys. Rev. Lett.**, 100:142001.
- Christenson, J. H., Hummel, E., Kreiter, G. A., Sculli, J., and Yamin, P. (1985). Limits on charm production in hadronic interactions near threshold. **Phys. Rev. Lett.**, 55:154.
- Collins, P. D. B. (1971). Regge theory and particle physics. **Phys. Rept.**, 1:103–234.
- Dashen, R. F., Jenkins, E. E., and Manohar, A. V. (1995). Spin flavor structure of large- $N_c$  baryons. **Phys. Rev. D**, 51:3697–3727.

- Donnachie, S., Dosch, H. G., Nachtmann, O., and Landshoff, P. (2004). **Pomeron physics and QCD**, volume 19. Cambridge University Press.
- Dover, C. B., Gutsche, T., Maruyama, M., and Faessler, A. (1992). The Physics of nucleon - anti-nucleon annihilation. **Prog. Part. Nucl. Phys.**, 29:87–174.
- Ebert, D., Faustov, R. N., and Galkin, V. O. (2006). Masses of heavy tetraquarks in the relativistic quark model. **Phys. Lett. B**, 634:214–219.
- Ebert, D., Galkin, V. O., and Faustov, R. N. (1998). Mass spectrum of orbitally and radially excited heavy-light mesons in the relativistic quark model. **Phys. Rev. D**, 57:5663–5669. [Erratum: Phys.Rev.D 59, 019902 (1999)].
- Faessler, A., Khosonthongkee, K., Kobdaj, C., Liphirat, A., Suebka, P., and Yan, Y. (2010). Low-lying baryon decays in the  $^3P_0$  quark model. **J. Phys. G**, 37(11):115002.
- Fontoura, C. E., Haidenbauer, J., and Krein, G. (2017). SU(4) flavor symmetry breaking in D-meson couplings to light hadrons. **Eur. Phys. J. A**, 53(5):92.
- Frankfurt, L., Strikman, M., Larionov, A., Lehrach, A., Maier, R., van Hees, H., Spieles, C., Vovchenko, V., and Stöcker, H. (2020). **Novel physics opportunities at the HESR-Collider with PANDA at FAIR.**
- Gasser, J. (1987). Chiral perturbation theory and effective Lagrangians. **Nucl. Phys. B**, 279:65–79.
- Gasser, J. and Leutwyler, H. (1984). Chiral perturbation theory to one loop. **Annals Phys.**, 158:142.

- Georgi, H. (1990). An effective field theory for heavy quarks at low-energies. **Phys. Lett. B**, 240:447–450.
- Glozman, L. Y. (2004). Chiral multiplets of excited mesons. **Phys. Lett. B**, 587:69–77.
- Godfrey, S. and Isgur, N. (1985). Mesons in a relativized quark model with chromodynamics. **Phys. Rev. D**, 32:189–231.
- Goritschnig, A. T., Kroll, P., and Schweiger, W. (2009). Proton-antiproton annihilation into a  $\Lambda_c^+ \bar{\Lambda}_c^-$  Pair. **Eur. Phys. J. A**, 42:43–62.
- Gupta, S. N. and Johnson, J. M. (1995). Quantum chromodynamic potential model for light heavy quarkonia and the heavy quark effective theory. **Phys. Rev. D**, 51:168–175.
- Haberzettl, H., Bennhold, C., Mart, T., and Feuster, T. (1998). Gauge-invariant tree-level photoproduction amplitudes with form factors. **Phys. Rev. C**, 58(1):R40–R44.
- Haidenbauer, J., Hippchen, T., Holinde, K., Holzenkamp, B., Mull, V., and Speth, J. (1992). The Reaction  $p\bar{p} \rightarrow \bar{\Lambda}\Lambda$  in the meson exchange picture. **Phys. Rev. C**, 45:931–946.
- Haidenbauer, J. and Krein, G. (2017). Production of charmed baryons in  $\bar{p}p$  collisions close to their thresholds. **Phys. Rev. D**, 95(1):014017.
- Hosaka, A., Iijima, T., Miyabayashi, K., Sakai, Y., and Yasui, S. (2016). Exotic hadrons with heavy flavors: X, Y, Z, and related states. **PTEP**, 2016(6):062C01.



- Isgur, N. and Karl, G. (1979). Ground State Baryons in a Quark Model with Hyperfine Interactions. **Phys. Rev. D**, 20:1191–1194.
- Isgur, N. and Paton, J. E. (1985). A flux tube model for hadrons in QCD. **Phys. Rev. D**, 31:2910.
- Jenkins, E. E. (1998). Large- $N_c$  baryons. **Ann. Rev. Nucl. Part. Sci.**, 48:81–119.
- Kaidalov, A. B. and Volkovitsky, P. E. (1994). Binary reactions in  $\bar{p}p$  collisions at intermediate-energies. **Z. Phys. C**, 63:517–524.
- Khodjamirian, A., Klein, C., Mannel, T., and Wang, Y. M. (2012). How much charm can  $\bar{P}$ ANDA produce? **Eur. Phys. J. A**, 48:31.
- Kim, S. H., Hosaka, A., Kim, H. C., and Noumi, H. (2015). Production of strange and charmed baryons in pion induced reactions. **Phys. Rev. D**, 92(9):094021.
- Kim, S. H., Hosaka, A., Kim, H. C., and Noumi, H. (2016). Pion induced reactions for the study of charmed baryons. **JPS Conf. Proc.**, 10:042004.
- Kittimanapun, K., Yan, Y., Khosonthongkee, K., Kobdaj, C., and Suebka, P. (2009).  $e^+e^- \rightarrow \omega\pi$  reaction and  $\rho(1450)$  and  $\rho(1700)$  mesons in a quark model. **Phys. Rev. C**, 79:025201.
- Koch, V. (1997). Aspects of chiral symmetry. **Int. J. Mod. Phys. E**, 6:203–250.
- Kroll, P., Quadder, B., and Schweiger, W. (1989). Exclusive production of heavy flavors in proton-antiproton annihilation. **Nucl. Phys. B**, 316:373–390.

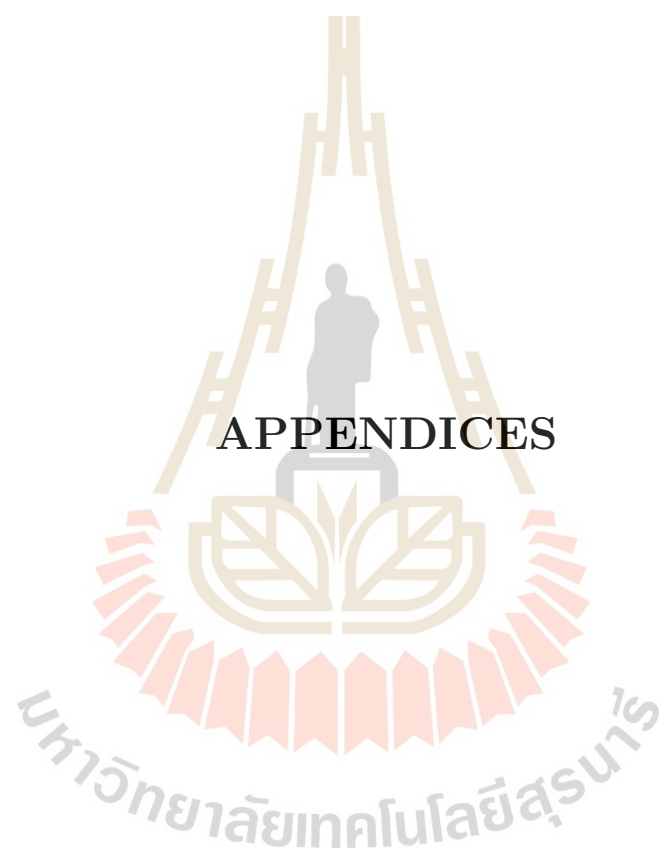
- Larionov, A. B. and Lenske, H. (2017). Distillation of scalar exchange by coherent hypernucleus production in antiproton–nucleus collisions. **Phys. Lett. B**, 773:470–475.
- Lebed, R. F. (1999). Phenomenology of large- $N_c$  QCD. **Czech. J. Phys.**, 49:1273–1306.
- Liao, X. and Manke, T. (2002). Excited charmonium spectrum from anisotropic lattices.
- Limphirat, A., Kobdaj, C., Suebka, P., and Yan, Y. (2010). Decay widths of ground-state and excited  $\Xi_b$  baryons in a nonrelativistic quark model. **Phys. Rev. C**, 82:055201.
- Limphirat, A., Sreethawong, W., Khosonthongkee, K., and Yan, Y. (2014). Reaction  $e^+e^- \rightarrow \bar{D}D$  and  $\psi'$  mesons. **Phys. Rev. D**, 89(5):054030.
- Liu, X., Yu, Y. M., Zhao, S. M., and Li, X. Q. (2006). Study on decays of  $D_{sJ}^*(2317)$  and  $D_{sJ}(2460)$  in terms of the CQM model. **Eur. Phys. J. C**, 47:445–452.
- Liu, Z. Q., Shen, C. P., Yuan, C. Z., Adachi, I., Aihara, H., Asner, D. M., Aulchenko, V., Aushev, T., Aziz, T., Bakich, A. M., Bala, A., Belous, K., Bhardwaj, V., Bhuyan, B., Bischofberger, M., et al. (2013). Study of  $e^+e^- \rightarrow \pi^+\pi^- J/\psi$  and observation of a charged charmoniumlike state at Belle. **Phys. Rev. Lett.**, 110:252002. [Erratum: Phys.Rev.Lett. 111, 019901 (2013)].
- Luty, M. A. and March-Russell, J. (1994). Baryons from quarks in the  $1/N$  expansion. **Nucl. Phys. B**, 426:71–93.

- Lutz, M. F. M. and Semke, A. (2011). Large- $N_c$  operator analysis of 2-body meson-baryon counterterms in the chiral Lagrangian. **Phys. Rev. D** 83:034008.
- Machleidt, R. and Entem, D. R. (2011). Chiral effective field theory and nuclear forces. **Phys. Rept.**, 503:1–75.
- Maiani, L., Piccinini, F., Polosa, A. D., and Riquer, V. (2005). Diquark-antidiquarks with hidden or open charm and the nature of X(3872). **Phys. Rev. D**, 71:014028.
- Manohar, A. V. and Wise, M. B. (2000). **Heavy quark physics**, volume 10.
- McNeile, C., Michael, C., and Pennanen, P. (2002). Hybrid meson decay from the lattice. **Phys. Rev. D**, 65:094505.
- Micu, L. (1969). Decay rates of meson resonances in a quark model. **Nucl. Phys. B**, 10:521–526.
- Morino, Y., Nakano, T., Noumi, H., Shirotori, K., Sugaya, Y., and Yamaga, T. (2012). Charmed baryon spectroscopy via the  $(\pi^-, D^{*-})$  reaction. **J-PARC P50 proposal**.
- Muhm, A., Gutsche, T., Thierauf, R., Yan, Y., and Faessler, A. (1996).  $p$  anti- $p$  annihilation into two mesons in the quark annihilation model including final state interaction. **Nucl. Phys. A**, 598:285–317.
- Nagels, M. M., Rijken, T. A., and de Swart, J. J. (1979). Baryon-Baryon scattering in a one boson exchange potential approach. III. A Nucleon-Nucleon and Hyperon-Nucleon analysis including contributions of a nonet of scalar mesons. **Phys. Rev. D**, 20:1633.

- Nam, S. I., Hosaka, A., and Kim, H. C. (2005).  $\Lambda(1520, 3/2^-)$  photoproduction reaction via  $\gamma N \rightarrow K\Lambda(1520)$ . **Phys. Rev. D**, 71:114012.
- Neubert, M. (1994). Heavy quark symmetry. **Phys. Rept.**, 245:259–396.
- Nowak, M. A., Rho, M., and Zahed, I. (2004). Chiral doubling of heavy light hadrons: BABAR 2317 MeV/c<sup>2</sup> and CLEO 2463-MeV/c<sup>2</sup> discoveries. **Acta Phys. Polon. B**, 35:2377–2392.
- Okamoto, M., Aoki, S., Burkhalter, R., Ejiri, S., Fukugita, M., Hashimoto, S., Ishikawa, K. I., Ishizuka, N., Iwasaki, Y., Kanaya, K., Kaneko, T., Kuramashi, Y., Lesk, V., Nagai, K., Okawa, M., et al. (2002). Charmonium spectrum from quenched anisotropic lattice QCD. **Phys. Rev. D**, 65:094508.
- Pais, A. (1966). Dynamical symmetry in particle physics. **Rev. Mod. Phys.**, 38:215–255.
- Rijken, T. A., Stoks, V. G. J., and Yamamoto, Y. (1999). Soft core hyperon - nucleon potentials. **Phys. Rev. C**, 59:21–40.
- Samart, D., Nualchimplee, C., and Yan, Y. (2016). Combined heavy-quark symmetry and large- $N_c$  operator analysis for 2-body counterterms in the chiral Lagrangian with  $D$  mesons and charmed baryons. **Phys. Rev. D**, 93(11):116004.
- Sangkhakrit, T., Shim, S. I., Yan, Y., and Hosaka, A. (2022). Charmed baryon pair production in proton-antiproton collisions in effective Lagrangian and Regge approaches. **Eur. Phys. J. A**, 58(2):32.
- Scherer, S. and Schindler, M. R. (2012). **A Primer for chiral perturbation theory**, volume 830.

- Semke, A. (2010). **On the quark-mass dependence of baryon ground-state masses**. PhD thesis, Darmstadt, Tech. Hochsch.
- Shim, S. I., Hosaka, A., and Kim, H. C. (2019). Strange and charmed baryon productions with an instanton interaction. **JPS Conf. Proc.**, 26:022030.
- Shim, S. I., Hosaka, A., and Kim, H. C. (2020). Heavy baryon production with an instanton interaction. **PTEP**, 2020(5):053D01.
- Shyam, R. and Lenske, H. (2014). Reaction  $\bar{p}p \rightarrow \bar{\Lambda}_c^- \Lambda_c^+$  within an effective Lagrangian model. **Phys. Rev. D**, 90(1):014017.
- Sreethawong, W., Xu, K., and Yan, Y. (2015). Exclusion of  $c\bar{c}$  interpretation for X(3940). **J. Phys. G**, 42(2):025001.
- Swanson, E. S. (2006). The New heavy mesons: a status report. **Phys. Rept.**, 429:243–305.
- 't Hooft, G. (1974a). A planar diagram theory for strong interactions. **Nucl. Phys. B**, 72:461.
- 't Hooft, G. (1974b). A two-dimensional model for mesons. **Nuclear Physics B** 75(3): 461 – 470.
- Titov, A. I. and Kampfer, B. (2008). Exclusive charm production in  $\bar{p}p$  collisions at  $\sqrt{s} \lesssim 15$  GeV. **Phys. Rev. C**, 78:025201.
- Weinberg, S. (1979). Phenomenological Lagrangians. **Physica A**, 96(1-2):327–340.
- Wise, M. B. (1993). Combining chiral and heavy quark symmetry. In *CCAST Symposium on Particle Physics at the Fermi Scale*.

- Witten, E. (1979). Baryons in the  $\frac{1}{N}$  expansion. **Nuclear Physics B** 160(1): 57–115.
- Xu, K., Kaewsnod, A., Zhao, Z., Liu, X. Y., Srisuphaphon, S., Limphirat, A., and Yan, Y. (2020). Pentaquark components in low-lying baryon resonances. **Phys. Rev. D**, 101(7):076025.
- Yan, T. M., Cheng, H. Y., Cheung, C. Y., Lin, G. L., Lin, Y. C., and Yu, H. L. (1992). Heavy-quark symmetry and chiral dynamics. **Phys. Rev. D**, 46:1148–1164.
- Yan, Y., Kobdaj, C., Suebka, P., Zheng, Y. M., Faessler, A., Gutsche, T., and Lyubovitskij, V. E. (2005). Electron-positron annihilation into hadron-antihadron pairs. **Phys. Rev. C**, 71:025204.
- Yu, G. L., Guan, R. H., and Wang, Z. G. (2019). Analysis of the strong vertices of  $\Sigma_c ND^*$  and  $\Sigma_b NB^*$  in QCD sum rules. **Int. J. Mod. Phys. A**, 33(36):1850217.



APPENDICES

# APPENDIX A

## CHIRAL POWER COUNTING OF MATTER FIELDS

The self-interactions of Goldstone bosons as well as their interactions with external fields are successfully described in ChPT for mesons. In general, matter fields such as baryons and heavy mesons can also be incorporated as we have already presented in Chapter II. Unlike Goldstone bosons, these matter fields are not massless in the chiral limit, where  $m_q \rightarrow \infty$ . This means, the four-momentum cannot be treated as a small quantity as those of Goldstone fields. Therefore, the inclusion of the matter fields requires the additional power counting rules. In fact, spatial three-momentum of the matter field can be regarded as a small quantity.

For example, the four momentum  $p$  of the matter field can be written into the sum of the two components, i.e.  $p = (m, \mathbf{0}) + (E - m, \mathbf{p})$ . In the chiral limit, the first term is larger than the second one. Therefore, the second term is counted as  $\mathcal{O}(q)$ , in which  $q$  denotes the ratio between spatial momenta or quark masses and cutoff or typical mass scales. The power counting rule for pseudoscalar D-meson is then given by,

$$D, \partial_\mu D \sim \mathcal{O}(q^0). \quad (\text{A.1})$$

For vector D-meson, the corresponding counting rule is

$$D_\mu, D_{\mu\nu} \sim \mathcal{O}(q^0). \quad (\text{A.2})$$

The relevant power counting rules of the bilinears  $\bar{\psi}\Gamma\psi$ ,  $\bar{\Psi}^\mu\Gamma\psi$ , and  $\bar{\Psi}^\mu\Gamma\Psi^\nu$  are



understood by evaluating the matrix elements of positive-energy solutions of the Dirac equation

$$\psi_{q,s}^+(x) = e^{-iq \cdot x} \sqrt{\frac{E_q + m}{2m}} \begin{pmatrix} 1 \\ \frac{\boldsymbol{\sigma} \cdot \mathbf{q}}{E_q + m} \end{pmatrix} \chi_s^{(1/2)}, \quad (\text{A.3})$$

and of those for Rarita-Schwinger equation

$$\Psi_{q,s}^{\mu+}(x) = e^{-iq \cdot x} \sqrt{\frac{E_q + m}{2m}} \begin{pmatrix} S^{\mu\dagger}(q) \\ S^{\mu\dagger}(q) \frac{\boldsymbol{\sigma} \cdot \mathbf{q}}{E_q + m} \end{pmatrix} \chi_s^{(3/2)}, \quad (\text{A.4})$$

with

$$\chi_1^{(1/2)} = \begin{pmatrix} 1 \\ 0 \end{pmatrix}, \chi_2^{(1/2)} = \begin{pmatrix} 0 \\ 1 \end{pmatrix}, E_q = \sqrt{q^2 + m^2}, \quad (\text{A.5})$$

and

$$\chi_1^{3/2} = \begin{pmatrix} 1 \\ 0 \\ 0 \\ 0 \end{pmatrix}, \chi_2^{3/2} = \begin{pmatrix} 0 \\ 1 \\ 0 \\ 0 \end{pmatrix}, \chi_3^{3/2} = \begin{pmatrix} 0 \\ 0 \\ 1 \\ 0 \end{pmatrix}, \chi_4^{3/2} = \begin{pmatrix} 0 \\ 0 \\ 0 \\ 1 \end{pmatrix}. \quad (\text{A.6})$$

The spin-transition matrices denoted by  $S^\mu(q)$  are explicitly written as

$$S^{0\dagger} = \frac{|\mathbf{q}|}{m} \begin{pmatrix} 0 & \sqrt{\frac{2}{3}} & 0 & 0 \\ 0 & 0 & \sqrt{\frac{2}{3}} & 0 \end{pmatrix}, S^{1\dagger} = \begin{pmatrix} -\frac{1}{\sqrt{2}} & 0 & \frac{1}{\sqrt{6}} & 0 \\ 0 & -\frac{1}{\sqrt{6}} & 0 & \frac{1}{\sqrt{2}} \end{pmatrix}, \quad (\text{A.7})$$

$$S^{2\dagger} = \begin{pmatrix} -\frac{i}{\sqrt{2}} & 0 & -\frac{i}{\sqrt{6}} & 0 \\ 0 & -\frac{i}{\sqrt{6}} & 0 & -\frac{i}{\sqrt{2}} \end{pmatrix}, S^{3\dagger} = \frac{E_q}{m} \begin{pmatrix} 0 & \sqrt{\frac{2}{3}} & 0 & 0 \\ 0 & 0 & \sqrt{\frac{2}{3}} & 0 \end{pmatrix}, \quad (\text{A.8})$$

In the low energy limit, the lower components of these plane-wave solutions are suppressed as  $\frac{|\mathbf{q}|}{m}$  with respect to the upper components. To analyze the momentum dependence of the bilinears, we divide the 16  $\Gamma$  matrices into two sets,  $\mathcal{E} = \{\mathcal{I}, \gamma_0, \gamma_i \gamma_5, \sigma_{ij}\}$  and  $\mathcal{O} = \{\gamma_i, \gamma_5, \gamma_0 \gamma_5, \sigma_{0j}\}$ , respectively. The matrices in  $\mathcal{O}$  couple large and small components while those in  $\mathcal{E}$  do the opposite. As a consequence, the counting rules for the bilinears  $\bar{\psi} \Gamma \psi$ ,  $\bar{\Psi}^\mu \Gamma \psi$ , and  $\bar{\Psi}^\mu \Gamma \Psi^\nu$  are given

as

$$1, \gamma_\mu, \gamma_\mu \gamma_5, \sigma_{\mu\nu} \sim \mathcal{O}(q^0), \gamma_5 \sim \mathcal{O}(q), \quad (\text{A.9})$$

where  $q$  denotes the spatial momentum.

In this appendix, we have derived the chiral power counting rules of our building blocks of the general chiral effective Lagrangian. These power counting rules are then applied to classify the relevant Lagrangians at a given order in  $q$ .



## APPENDIX B

### ISOSPIN MATRICES

Under  $SU(2)$  isospin symmetry, we usually represent the isotriplet fields  $\Sigma_c$  and  $\Sigma_c^*$  in their adjoint representations. Such representation can be written by employing a three dimensional basis composed of the isospin matrices. When the isotriplet state is coupled with doublet and anti-doublet states, it is convenient to represent it in terms of three isospin Pauli-matrices,

$$\tau_1 = \begin{pmatrix} 0 & 1 \\ 1 & 0 \end{pmatrix}, \tau_2 = \begin{pmatrix} 0 & -i \\ i & 0 \end{pmatrix}, \tau_3 = \begin{pmatrix} 1 & 0 \\ 0 & -1 \end{pmatrix}. \quad (\text{B.1})$$

In our case, we can represent the isotriplet state  $\Sigma_c$  as

$$\Sigma_c^{(t)} = \frac{1}{\sqrt{2}} \boldsymbol{\tau} \cdot \boldsymbol{\Sigma}_c = \begin{pmatrix} \Sigma_c^{(3)} & \Sigma_c^{(1)} + i\Sigma_c^{(2)} \\ \Sigma_c^{(1)} + i\Sigma_c^{(2)} & -\Sigma_c^{(3)} \end{pmatrix}, \quad (\text{B.2})$$

where the fundamental  $\Sigma_c$  fields are collected in  $\boldsymbol{\Sigma}_c = (\Sigma_c^{(1)}, \Sigma_c^{(2)}, \Sigma_c^{(3)})$  while  $\boldsymbol{\tau} = (\tau_1, \tau_2, \tau_3)$ . The transformations between the fundamental  $\Sigma_c$  fields and the eigenstates of the electric charge, the physical  $\Sigma_c$  fields, are given as

$$\Sigma_c^{++} = \frac{1}{\sqrt{2}} (\Sigma_c^{(1)} - i\Sigma_c^{(2)}), \quad (\text{B.3})$$

$$\Sigma_c^0 = \frac{1}{\sqrt{2}} (\Sigma_c^{(1)} + i\Sigma_c^{(2)}), \quad (\text{B.4})$$

$$\Sigma_c^+ = \Sigma_c^{(3)}. \quad (\text{B.5})$$

Therefore, the  $2 \times 2$  matrix  $\Sigma_c^{(t)}$  is written as,

$$\Sigma_c^{(t)} = \begin{pmatrix} \frac{1}{\sqrt{2}}\Sigma_c^+ & \Sigma_c^{++} \\ \Sigma_c^0 & -\frac{1}{\sqrt{2}}\Sigma_c^+ \end{pmatrix}. \quad (\text{B.6})$$

On the other hand, this representation becomes irrelevant when we couple it to the isobar state. Therefore, the adjoint representation of  $\Sigma_c$  field can be reinterpreted in terms of isospin transition matrices,

$$T_1 = \begin{pmatrix} -\frac{1}{\sqrt{2}} & 0 \\ 0 & -\frac{1}{\sqrt{6}} \\ \frac{1}{\sqrt{6}} & 0 \\ 0 & \frac{1}{\sqrt{2}} \end{pmatrix}, T_2 = \begin{pmatrix} \frac{i}{\sqrt{2}} & 0 \\ 0 & \frac{i}{\sqrt{6}} \\ \frac{i}{\sqrt{6}} & 0 \\ 0 & \frac{i}{\sqrt{2}} \end{pmatrix}, T_3 = \begin{pmatrix} 0 & 0 \\ \sqrt{\frac{2}{3}} & 0 \\ 0 & \sqrt{\frac{2}{3}} \\ 0 & 0 \end{pmatrix}, \quad (\text{B.7})$$

In this case, the  $4 \times 2$  matrix  $\Sigma_c^{(T)}$  is written by

$$\Sigma_c^{(T)} = \mathbf{T} \cdot \Sigma_c = \begin{pmatrix} -\Sigma_c^{++} & 0 \\ \sqrt{\frac{2}{3}}\Sigma_c^+ & -\frac{1}{\sqrt{3}}\Sigma_c^{++} \\ \frac{1}{\sqrt{3}}\Sigma_c^0 & \sqrt{\frac{2}{3}}\Sigma_c^+ \\ 0 & \Sigma_c^0 \end{pmatrix}, \quad (\text{B.8})$$

with  $\mathbf{T} = (T_1, T_2, T_3)$ . Originally, these matrices are constructed in the derivation of spin- $\frac{3}{2}$  Rarita-Schwinger fields. More details can be found from Ref. (Semke, 2010).

# APPENDIX C

## REGGE PARAMETERS

In Regge theory, the transition amplitude in the Regge representation has already been introduced in Chapter V. There are two model parameters: Regge trajectory  $\alpha(t)$  and scaling parameter  $s_0$ . In this appendix, the evaluations of these parameters will be briefly summarized. More information regarding the evaluations of Regge trajectories can be found in Ref. (Brisudova et al., 2000). For QGSM, the detailed information is provided in Ref. (Kaidalov and Volkovitsky, 1994).

### C.1 Regge trajectories

We focus our discussion with meson trajectories since they have been employed to calculate production rates of various strange and charmed baryons. In general, we can write the Regge trajectory  $\alpha(t)$  in the nonlinear representation

$$\alpha(t) = \alpha(0) + \gamma \left[ \sqrt{T} - \sqrt{T-t} \right], \quad (\text{C.1})$$

where the parameter  $\gamma$  denotes an universal slope while the scale parameter is written as  $T$ . In the diffractive region where  $-t \ll T$ , the expression in Eq. (C.1) is approximated as

$$\alpha(t) = \alpha(0) + \alpha' t, \quad (\text{C.2})$$

with the corresponding slope  $\alpha' = \frac{\gamma}{2\sqrt{T}}$ .

The trajectory intercepts and slopes are related by (Kaidalov and Volkovit-

sky, 1994; Brisudova et al., 2000)

$$2\alpha_{i\bar{j}}(0) = \alpha_{i\bar{i}}(0) + \alpha_{j\bar{j}}(0), \quad (\text{C.3})$$

$$2[\alpha'_{i\bar{j}}]^{-1} = [\alpha'_{i\bar{i}}]^{-1} + [\alpha'_{j\bar{j}}]^{-1}, \quad (\text{C.4})$$

where  $i, j$  ( $\bar{i}, \bar{j}$ ) denote quark (antiquark) flavor. First, we consider the trajectory of  $\rho$ -meson. The trajectory intercept which agrees with relevant evidences is given as  $\alpha_\rho(0) = 0.55$  (Brisudova et al., 2000). By using the mass-spin relations of  $\rho$  and  $\rho_3$ ,

$$\alpha_\rho(m_\rho^2) = 1, m_\rho = 769.0 \pm 0.9 \text{ MeV}, \quad (\text{C.5})$$

$$\alpha_\rho(m_{\rho_3}^2) = 3, m_{\rho_3} = 1688.8 \pm 2.1 \text{ MeV}, \quad (\text{C.6})$$

the following parameters are consequently extracted

$$\gamma = 3.65 \pm 0.05 \text{ GeV}^{-1}, \sqrt{T_\rho} = 2.46 \pm 0.03 \text{ GeV}. \quad (\text{C.7})$$

Then, the parameters of  $K^*$  trajectory are obtained by using the following relations

$$\alpha_{K^*}(m_{K^*}^2) = 1, m_{K^*} = 896.1 \pm 0.3 \text{ MeV}, \quad (\text{C.8})$$

$$\alpha_{K^*}(m_{K_3^*}^2) = 3, m_{K_3^*} = 1776 \pm 7 \text{ MeV}, \quad (\text{C.9})$$

and the universal slope  $\gamma$ , which implies that

$$\alpha_{K^*}(0) = 0.414 \pm 0.006, \sqrt{T_{K^*}} = 2.58 \pm 0.03 \text{ GeV}. \quad (\text{C.10})$$

By using relations in Eqs. (C.3) to (C.4), the parameters for  $\phi$  are then extracted. Therefore, trajectories for those containing charm quarks can also be extracted by

using the universal slope  $\gamma$  and masses of the associated states. The parameters for relevant meson trajectories are summarized in Table C.1

**Table C.1** Parameters of corresponding meson trajectories for strangeness and charm productions from  $p\bar{p}$  reactions

Trajectory	$\alpha(0)$	$\sqrt{T}$ (GeV)	$\alpha'$ (GeV <sup>-2</sup> )
$\pi$	-0.0118	2.82	0.647
$K$	-0.151	2.96	0.617
$\eta_s$	-0.291	3.10	0.606
$D$	-1.61105	4.16	0.439
$\eta_c$	-3.2103	5.49	0.332
$\rho$	0.55	2.46	0.742
$K^*$	0.414	2.58	0.707
$\phi$	0.27	2.70	0.675
$D^*$	-1.02	3.91	0.467
$J/\psi$	-2.60	5.36	0.340

## C.2 Scaling parameters

In Kaidalov's QGSM, the scaling parameter for the elastic scattering  $ab \rightarrow ab$  is calculated in terms of transverse masses of the quarks in the hadrons  $a$  and  $b$  as

$$s^{ab} = \left( \sum_j m_{\perp j} \right)_a \left( \sum_k m_{\perp k} \right)_b, \quad (\text{C.11})$$

where  $m_{\perp j}$  denotes the transverse mass of the constituent quark  $j$ , in which  $m_{\perp q} = 0.5$  GeV,  $m_{\perp s} = 0.6$  GeV, and  $m_{\perp c} = 1.6$  GeV. Therefore, the following scaling parameters are obtained,

$$s^{p\bar{p}} = 2.25 \text{ GeV}^2 \quad (\text{C.12})$$

$$s^{\Lambda\bar{\Lambda}} = s^{\Sigma\bar{\Lambda}} = s^{\Sigma\bar{\Sigma}} = 2.56 \text{ GeV}^2 \quad (\text{C.13})$$

$$s^{\Lambda_c\bar{\Lambda}_c} = s^{\Sigma_c\bar{\Lambda}_c} = s^{\Sigma_c\bar{\Sigma}_c} = 6.76 \text{ GeV}^2 \quad (\text{C.14})$$

From the factorization of the inelastic scattering amplitude in the  $s$ -channel, the relations between the scaling factors of inelastic scattering ( $ab \rightarrow cd$ ) and those of elastic scatterings ( $ab \rightarrow ab$  and  $cd \rightarrow cd$ ) are

$$\left(s_p^{ab \rightarrow cd}\right)^{2\alpha_{ij}(0)} = \left(s^{ab}\right)^{\alpha_{ii}(0)} \left(s^{cd}\right)^{\alpha_{jj}(0)}, \quad (\text{C.15})$$

$$\left(s_v^{ab \rightarrow cd}\right)^{2[\alpha_{ij}(0)-1]} = \left(s^{ab}\right)^{\alpha_{ii}(0)-1} \left(s^{cd}\right)^{\alpha_{jj}(0)-1}, \quad (\text{C.16})$$

where the corresponding exchanged trajectories are identified by the subscripts  $p$  (for pseudoscalar meson) and  $v$  (for vector meson). Therefore, the scaling parameters for various strangeness productions are evaluated from

$$\left(s_K^{p\bar{p} \rightarrow \Lambda\bar{\Lambda}}\right)^{2\alpha_K(0)} = \left(s^{p\bar{p}}\right)^{\alpha_\pi(0)} \left(s^{\Lambda\bar{\Lambda}}\right)^{\alpha_{\eta_s}(0)}, \quad (\text{C.17})$$

$$\left(s_K^{p\bar{p} \rightarrow \Sigma\bar{\Lambda}}\right)^{2\alpha_K(0)} = \left(s^{p\bar{p}}\right)^{\alpha_\pi(0)} \left(s^{\Sigma\bar{\Lambda}}\right)^{\alpha_{\eta_s}(0)}, \quad (\text{C.18})$$

$$\left(s_K^{p\bar{p} \rightarrow \Sigma\bar{\Sigma}}\right)^{2\alpha_K(0)} = \left(s^{p\bar{p}}\right)^{\alpha_\pi(0)} \left(s^{\Sigma\bar{\Sigma}}\right)^{\alpha_{\eta_s}(0)}, \quad (\text{C.19})$$

$$\left(s_{K^*}^{p\bar{p} \rightarrow \Lambda\bar{\Lambda}}\right)^{2(\alpha_{K^*}(0)-1)} = \left(s^{p\bar{p}}\right)^{\alpha_\rho(0)-1} \left(s^{\Lambda\bar{\Lambda}}\right)^{\alpha_\phi(0)-1}, \quad (\text{C.20})$$

$$\left(s_{K^*}^{p\bar{p} \rightarrow \Sigma\bar{\Lambda}}\right)^{2(\alpha_{K^*}(0)-1)} = \left(s^{p\bar{p}}\right)^{\alpha_\rho(0)-1} \left(s^{\Sigma\bar{\Lambda}}\right)^{\alpha_\phi(0)-1}, \quad (\text{C.21})$$

$$\left(s_{K^*}^{p\bar{p} \rightarrow \Sigma\bar{\Sigma}}\right)^{2(\alpha_{K^*}(0)-1)} = \left(s^{p\bar{p}}\right)^{\alpha_\rho(0)-1} \left(s^{\Sigma\bar{\Sigma}}\right)^{\alpha_\phi(0)-1}. \quad (\text{C.22})$$

In case of charm productions, the relevant scaling parameters are given from

$$\left(s_D^{p\bar{p} \rightarrow \Lambda_c\bar{\Lambda}_c}\right)^{2\alpha_D(0)} = \left(s^{p\bar{p}}\right)^{\alpha_\pi(0)} \left(s^{\Lambda_c\bar{\Lambda}_c}\right)^{\alpha_{\eta_c}(0)}, \quad (\text{C.23})$$

$$\left(s_D^{p\bar{p} \rightarrow \Sigma_c\bar{\Lambda}_c}\right)^{2\alpha_D(0)} = \left(s^{p\bar{p}}\right)^{\alpha_\pi(0)} \left(s^{\Sigma_c\bar{\Lambda}_c}\right)^{\alpha_{\eta_c}(0)}, \quad (\text{C.24})$$

$$\left(s_D^{p\bar{p} \rightarrow \Sigma_c\bar{\Sigma}_c}\right)^{2\alpha_D(0)} = \left(s^{p\bar{p}}\right)^{\alpha_\pi(0)} \left(s^{\Sigma_c\bar{\Sigma}_c}\right)^{\alpha_{\eta_c}(0)}, \quad (\text{C.25})$$



$$\left(s_{D^*}^{p\bar{p} \rightarrow \Lambda_c \bar{\Lambda}_c}\right)^{2(\alpha_{D^*}(0)-1)} = \left(s^{p\bar{p}}\right)^{\alpha_\rho(0)-1} \left(s^{\Lambda_c \bar{\Lambda}_c}\right)^{\alpha_{J/\psi}(0)-1}, \quad (\text{C.26})$$

$$\left(s_{D^*}^{p\bar{p} \rightarrow \Sigma_c \bar{\Lambda}_c}\right)^{2(\alpha_{D^*}(0)-1)} = \left(s^{p\bar{p}}\right)^{\alpha_\rho(0)-1} \left(s^{\Sigma_c \bar{\Lambda}_c}\right)^{\alpha_{J/\psi}(0)-1}, \quad (\text{C.27})$$

$$\left(s_{D^*}^{p\bar{p} \rightarrow \Sigma_c \bar{\Sigma}_c}\right)^{2(\alpha_{D^*}(0)-1)} = \left(s^{p\bar{p}}\right)^{\alpha_\rho(0)-1} \left(s^{\Sigma_c \bar{\Sigma}_c}\right)^{\alpha_{J/\psi}(0)-1}. \quad (\text{C.28})$$

By employing the intercepts of corresponding trajectories and elastic scaling parameters, the following results for strangeness and charm productions are obtained

$$s_K = s_K^{p\bar{p} \rightarrow \Lambda \bar{\Lambda}} = s_K^{p\bar{p} \rightarrow \Sigma \bar{\Lambda}} = s_K^{p\bar{p} \rightarrow \Sigma \bar{\Sigma}} = 2.42 \text{ GeV}^2, \quad (\text{C.29})$$

$$s_{K^*} = s_{K^*}^{p\bar{p} \rightarrow \Lambda \bar{\Lambda}} = s_{K^*}^{p\bar{p} \rightarrow \Sigma \bar{\Lambda}} = s_{K^*}^{p\bar{p} \rightarrow \Sigma \bar{\Sigma}} = 2.45 \text{ GeV}^2, \quad (\text{C.30})$$

$$s_D = s_D^{p\bar{p} \rightarrow \Lambda_c \bar{\Lambda}_c} = s_D^{p\bar{p} \rightarrow \Sigma_c \bar{\Lambda}_c} = s_D^{p\bar{p} \rightarrow \Sigma_c \bar{\Sigma}_c} = 5.46 \text{ GeV}^2, \quad (\text{C.31})$$

$$s_{D^*} = s_{D^*}^{p\bar{p} \rightarrow \Lambda_c \bar{\Lambda}_c} = s_{D^*}^{p\bar{p} \rightarrow \Sigma_c \bar{\Lambda}_c} = s_{D^*}^{p\bar{p} \rightarrow \Sigma_c \bar{\Sigma}_c} = 6.01 \text{ GeV}^2. \quad (\text{C.32})$$

# CURRICULUM VITAE

**NAME** Mr. Thanat Sangkhakrit  
**DATE OF BIRTH** April 2, 1991  
**PLACE OF BIRTH** Bangkok, Thailand  
**E-MAIL** tanattosan@outlook.jp

## EDUCATION

Doctor of Philosophy (2013 - present)

School of Physics, Suranaree University of Technology, Nakhon Ratchasima,  
Thailand

Supervisors: Prof. Dr. Yupeng Yan, Prof. Dr. Atsushi Hosaka,  
Dr. Daris Samart, and Dr. Nopmanee Supanam

Bachelor of Science (2009 - 2013)

Department of Physics, Srinakharinwirot University, Bangkok, Thailand

Supervisor: Asst. Prof. Dr. Suphot Musiri

## PUBLICATIONS

- [1] Sangkhakrit, T., Shim, S.I., Yan, Y. and Hosaka A., “**Charmed baryon pair production in proton-antiproton collisions in effective Lagrangian and Regge approaches**”, Eur. Phys. J. A **58** (2022) 32
- [2] Sangkhakrit, T., Kaewsnod, A., Sreethawong, W., Suyuporn, T., Supanam, N., Samart D. and Yan, Y., “**Estimation of coupling constants for  $D$ -meson, charmed, and light baryons in effective Lagrangian approach and quark model**”, Eur. Phys. J. A **59** (2023) 24